NTNU
Norwegian University of
Science and Technology

Losses and Inductive Parameters in Subsea Power Cables

Ronny Stølan

Master of Science in Electric Power Engineering
Submission date: July 2009
Supervisor: Arne Nysveen, ELKRAFT
Co-supervisor: Jarle Bremnes, Nexans

Norwegian University of Science and Technology
Department of Electric Power Engineering

Problem Description

Detailed knowledge of the magnetic field and its effects are essential for design and analysis of subsea cables. In recent years the market for subsea cables supplying electric power to subsea process facilities such as booster- and water injection pumps has been growing steadily. Tailor made cables for such application is a focus area for Nexans Norway. The umbilical supplying power to these units may comprises steel tubes and signal cables in addition to the power cable itself. The magnetic field distribution is complex, and detailed analysis is needed for calculating the different cable parameters. The object is to calculate and measure cable parameters at nominal frequency and for harmonics (from a frequency converter). The calculations will apply finite element analysis to be verified by measurements on specific cables. These measurements are to be conducted at Nexans Norway in Halden. Of special interest is the cable armoring and armoring permeability.
More specific, the master thesis includes:
- FEM calculations on fabricated cables. Comparison with measurements
- Establish a test setup for measurement of armouring losses in test cables
- Measurements of losses in the cable armouring including determine the permeability for applied steel qualities.
- Compare parameters for simplified IEC tube representation of the armouring with read individual strand armouring.

Further details to be clarified with the supervisors during the project work.

Assignment given: 02. February 2009
Supervisor: Arne Nysveen, ELKRAFT

NORGES TEKNISK-NATURVITENSKAPELIGE UNIVERSITET

NTNU

M A S T E R O P P G A V E

Kandidatens navn	: Ronny Stølan
Fag	: **ELKRAFTTEKNIKK**
Oppgavens tittel (norsk)	: Tap og induktive parametre i subsea kraftkabler
Oppgavens tittel (engelsk)	: Losses and inductive parameters in subsea power cables

Oppgavens tekst:

Detailed knowledge of the magnetic field and its effects are essential for design and analysis of subsea cables. In recent years the market for subsea cables supplying electric power to subsea process facilities such as booster- and water injection pumps has been growing steadily. Tailor made cables for such application is a focus area for Nexans Norway AS. The umbilical supplying power to these units may comprises steel tubes and signal cables in addition to the power cable itself.

The magnetic field distribution is complex, and detailed analysis is needed for calculating the different cable parameters. The object is to calculate and measure cable parameters at nominal frequency and for harmonics (from a frequency converter). The calculations will apply finite element analysis to be verified by measurements on specific cables. These measurements are to be conducted at Nexans Norway in Halden. Of special interest is the cable armoring and the magnetic permeability of the steel wires.

More specific, the master thesis includes:
- FEM calculations on fabricated cables. Comparison with measurements
- Establish a test setup for measurement of armouring losses in test cables
- Measurements of losses in the cable armouring including determine the permeability for applied steel qualities.
- Compare parameters for simplified IEC tube representation of the armouring with actual individual wires.

Further details to be clarified with the supervisors during the project work.

Oppgaven gitt	: 2. februar 2009
Oppgaven revidert:	: 10. juni 2009
Besvarelsen leveres innen	: 29. juni 2009
Besvarelsen levert	:
Utført ved (institusjon, bedrift)	: Inst. for elkraftteknikk/NTNU
Kandidatens veiledere	: Arne Nysveen Jarle Bremnes (Nexans Norway)
Faglærer	: Professor Arne Nysveen

Trondheim, 10. juni 2009

Arne Nysveen

faglærer

Preface

Research on the topics of this thesis commenced during a summer job at Nexans Norway AS cable factory in Halden in 2008. Results of tests performed at Nexans and NTNU over the last year, are presented.

I owe a number of people a great dept of gratitude for their assistance and guidance during the study of this thesis:

Jarle Bremnes at Nexans for an outstanding cooperation during the summer job and tests at the factory, and the considerable amount of help and guidance I have receive.

Arne Nysveen for his role as an excellent supervisor.

All the people at the service laboratory and electromechanical workshop for their support with the tests conducted at the laboratories of NTNU.

Thank you!

Trondheim, July 20th 2009

Ronny André Stølan

Ronny André Stølan

Summary

Four samples of galvanized steel armour for sub sea power cables are tested with an electric steel tester. The samples exhibit different remanence magnetization and permeability. The effects of permeability on loss in sub sea cables is found to be insignificant. Slight increase of conductor inductance due to increase in permeability of armour wires is observed.

Mutual cancellation of inductance between circuits that are twisted opposite to each other, or with respect to one circuit, is confirmed with laboratory tests and measurements on full scale sub sea power cables.

The parameters of one cable is calculated using IEC's analytical approach and found to be inaccurate for conductor resistance. The Calculations places 22% of total cable loss in the armour. Measurements on two sub sea cables and analysis using finite element method contradict the calculated armour loss.

Parameters for two sub sea power cables are calculated based on measurements performed on the actual cables. The calculated values are compared with values computed using finite element analysis. Derived physics from laboratory experiments and measurements on the cables is applied in finite element analysis and found to be accurate compared with calculated values from measurements and computed values using Flux 2.5D.

Contents

List of Figures

List of Tables

1 INTRODUCTION

1.1 Purpose of the Thesis

The purpose of this report is to examine the inductive parameters of power cables at nominal frequencies. Examine the effects of armour steel permeability on resistive loss and inductance. Determine correct physics for application in Finite Element Analysis based on experimental laboratory tests. Verify applied physics used in FEA of full scale power cables by comparing results with measured values. Determine accuracy of IEC's approach on calculating current rating and loss for power cables.

1.2 Background of the Thesis

Detailed knowledge of the magnetic field and its effects are essential for design and analysis of subsea cables. In recent years the market for subsea cables supplying electric power to subsea process facilities such as booster- and water injection pumps has been growing steadily. Tailor made cables for such application is a focus area for Nexans Norway AS. The umbilical supplying power to these units may comprises steel tubes and signal cables in addition to the power cable itself.

1.3 Scope of the Thesis

The main focus of this thesis is on physical tests and measurements. Rendering of published text and theory are therefore provided only to a small extent. Equations for use in Finite Element Analysis are derived through extensive experimental laboratory work. Results of measurements on real sub sea power cables, fabricated at Nexans Norway AS in Halden, are compared with values obtained by Finite Element Analysis. Analytical formulas provided by IEC in standard 60287-1-1 are used to calculate the current raring and loss for one of the power cables. Results are compared in a separate section, dedicated to discussions of the results and accuracy of measurements.

2 THEORY

2.1 Induced Voltage in Parallel Conductors

Two different cable circuits are illustrated in figure 1. The length of each cable is equal to one helix height. In figure 1a only the inner circuit is twisted. When applying a symmetrical three phase AC current to the green circuit, a net magnetic field will rotate with the same frequency as the applied current. Just by looking at the cross section of any of the two figures, it would seem that the conductors are parallel at a length into the plane. The rotating magnetic field would then induce a potential voltage difference over the length of the blue conductors. If the conductors are twisted, as figure 1a illustrates, the induced potential difference in the blue conductors would be a function of the sum of the magnetic field over one period, equal to zero. At any point in time, the blue conductors will experience the entire period of the magnetic potential, canceling out the potential difference of the conductors over one exact helix length.

Twisting both circuits in opposite direction, as figure 1b shows, the net induced voltage will cancel out over half a helix height, illustrated by the brown part of the blue conductor.

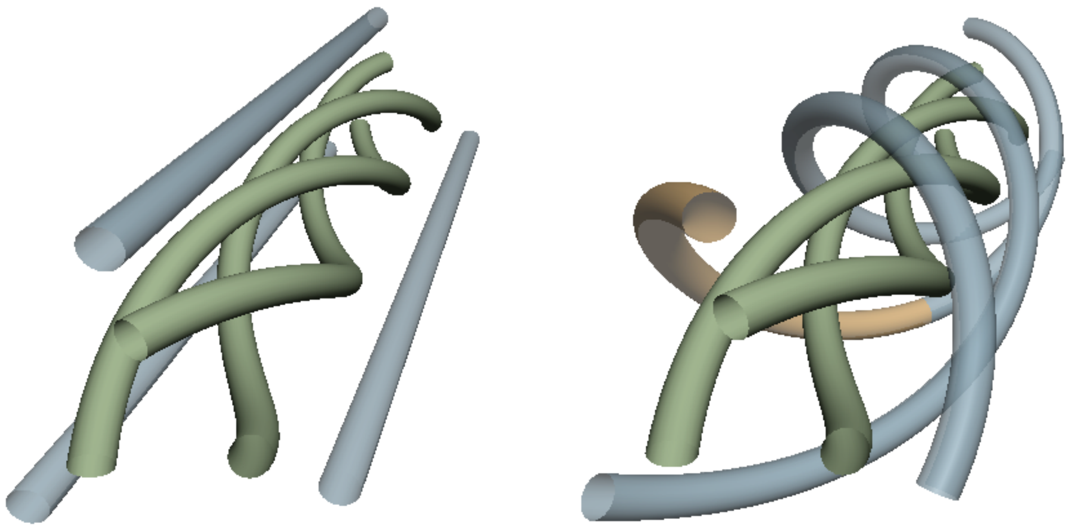

(a) Inner circuit twisted

(b) Both circuits twisted in opposite direction

Figure 1: Illustration of two cable circuits

2.2 Induced Loss in Armour

Losses in cable armouring can be divided into several categories, depending on the cable type, armour material and installation methods. Single core cables without metallic sheet generally have nonmagnetic armour, since the loss in steel wires would be to high. For single core cables with metallic sheet and nonmagnetic armour, the losses are calculated by using the combined resistance of the armour and the sheet in parallel. IEC standard 287 applies the same procedure for 2- and 3 core cables with metallic sheet and nonmagnetic armour. When the armour is magnetic, eddy current losses in armour is considered [1].

2.3 Magnetic Permeability

In ferromagnetic materials, such as iron, nickel, cobalt and alloys containing these elements, strong interactions between atomic magnetic moments cause them to line up parallel to each other in magnetic domains. Within each domain, nearly all of the atomic magnetic moments are parallel. The domain magnetization is randomly oriented when there is no externally applied field. In the presence of an external field $\vec{\mathrm{H}}$, the domains try to orient themselves parallel to the field. The domains that are magnetized in the direction of the field grow while the domains that are magnetized in the other directions shrink. As the external field is increased, a point is eventually reached at which nearly all of the magnetic moments in the ferromagnetic material are aligned parallel to the field. Increasing the external field beyond this point will only cause a minimal increase in the magnetization. This is called saturation magnetization. Figure 2 shows a magnetization curve for a ferromagnetic material.

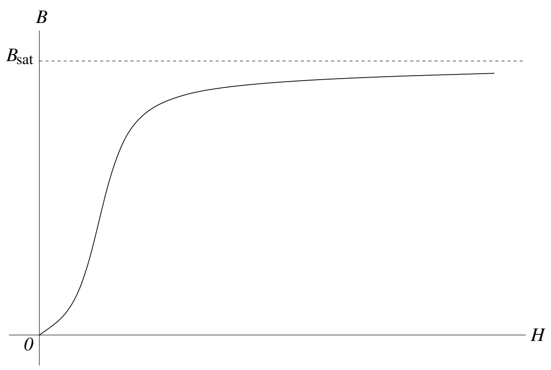

Figure 2: Magnetization curve for a ferromagnetic material. The magnetization approaches its saturation point as the external magnetic field increases.

When a ferromagnetic material is magnetized to saturation and the external field is reduced to zero, some magnetization remains. This is called magnetic remanence B_R. To reduce the magnetization to zero, an external magnetic field has to be applied in the reverse direction. This behavior is called hysteresis. Magnetizing and demagnetizing a material that has hysteresis involves the dissipation of energy and causes the material to heat up. Figure 3 shows three different examples of hysteresis loops. Since permanent magnets should have a high remanence and be hard to demagnetize, they are commonly made of materials that exhibit the characteristics of the hysteresis loop in figure 3a. A material with the hysteresis loop of figure 3b, could be used as magnetic storage media since it has high remanence and demagnetizes more easily. Materials for alternating current devices should have a narrow hysteresis loop with low remanence, like that of figure 3c, in order to reduce losses [2]. Using the external magnetic field strength $\vec{H}$ and the materials magnetic flux density $\vec{B}$, the permeability is defined as: $\mu = \frac{B}{H}$.

2.4 Caloric Theory

Caloric measurements are often used to determine the resistive losses of a system where electric quantities prove difficult to obtain. Assuming an adiabatic system – measuring the temperature increase or decrease over a specified period of time, together with the materials specific heat capacity and it's mass, an expression for the differential work is derived in equation (1). Dividing the work by the time it takes to cool down or heat up the material, the required power is obtained in equation (2) [3].

$$\Delta W = C_p m \Delta T \, [k\mathrm{J}] \tag{1}$$

$$P = \frac{\Delta W}{\Delta t} \, [\mathrm{W}] \tag{2}$$

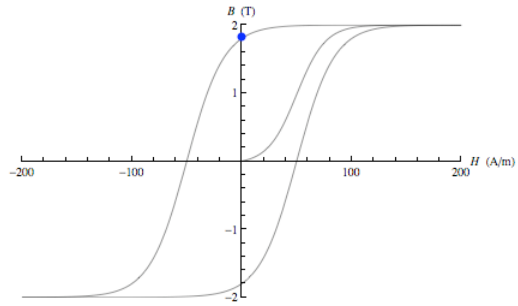

(a) wide hysteresis with high remanence.

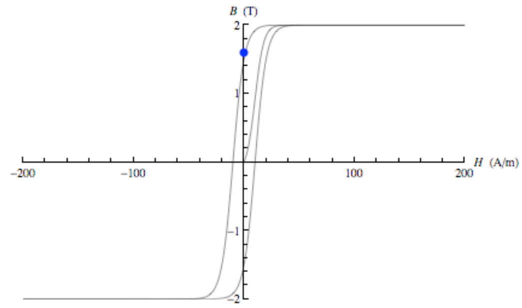

(b) Narrow hysteresis with high remanence.

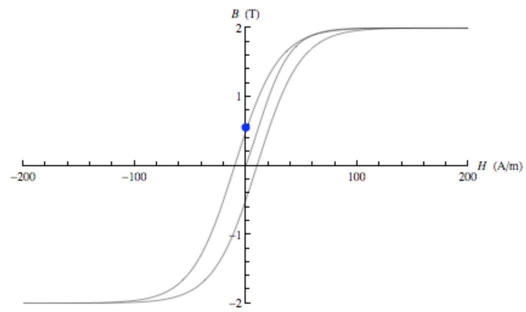

(c) Narrow hysteresis with low remanence

Figure 3: Hysteresis loops for three different applications. 3a has a characteristic typical of permanent magnet materials. Both 3b and 3c require smaller external field to demagnetize. Also, since 3b has a lower remanence, it's suitable for appliances such as transformer cores where zero hysteresis is desirable.

2.5 Thermal Radiation and Reflection

When using a thermal imaging camera, it is important to avoid the reflection of atmospheric disturbances from the test object, since this may cause inaccurate measurements. A piece of scotch tape is attached to the area where the temperature is to measured. All though the tape is transparent, it acts as a black body. In physics, a black body is an idealized object that absorbs all electromagnetic radiation that falls on it. No electromagnetic radiation passes through it and none is reflected. In figure 4, the camera is focused on a mirror, reflecting the radiated heat from an incandescent light bulb.

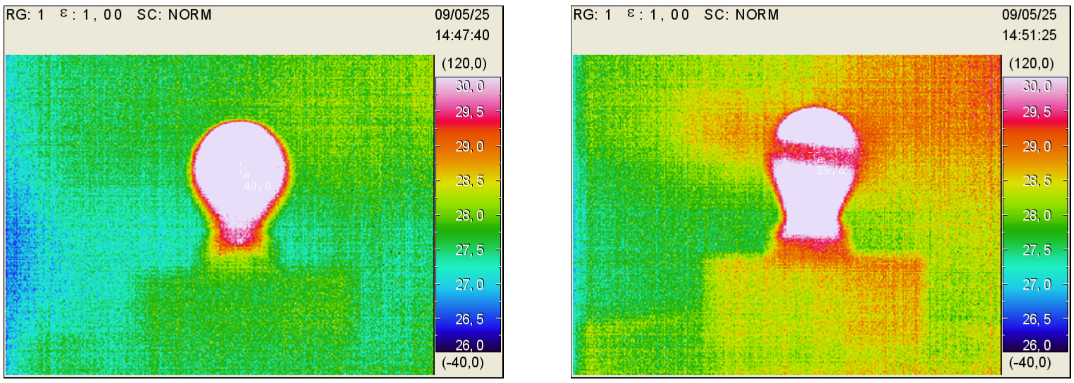

(a) Mirror reflection of incandescent light bulb. Reflection of thermal radiation: 40°C

(b) Mirror reflection of incandescent light bulb with a peace of scotch tape attached to the mirror. Reflection of thermal radiation: 29.6°C

Figure 4: Mirror reflections of incandescent light bulbs with and without attached tape

3 MEASUREMENTS

3.1 Magnetic Permeability of Armour Wires

Four different samples of galvanized steel armour wires for sub-sea power cables are tested in an electrical steel tester. One of the samples is of the same type as that used on TXVE 36 kV $6 \times 1 \times 95\,\mathrm{mm}^2$ in section 3.6.

3.1.1 Measuring equipment

The electrical steel tester consists of a laminated iron core and two coils, one exciter coil and one measuring coil, that wrap around the centre of the steel sample. The sample is tightly connected at both its ends to each leg of the laminated core. The resulting geometry resembles a three-legged transformer core with both high- and low voltage coils placed around the centre leg. In this case, the centre leg is the iron sample, and the coils are the exciter- and measuring coils, consisting of 900 turns each. Figure 5 illustrates the geometry of the core, coils and sample material. The sample material is exposed to a defined magnetic field that produces a magnetic flux in the sample. The induced voltage over the measuring coil is converted and integrated in a processor so that the desired output values can be calculated by the software.

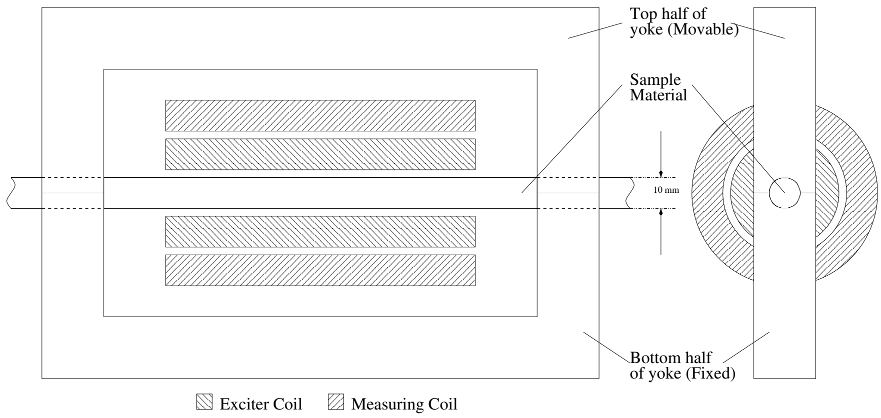

Figure 5: Electric steel tester with sample material

3.1.2 Armour wire samples

Samples used in the electric steel tester must have a diameter of exactly 10mm to ensure a good magnetic connection without any air gaps. The armour wire samples are all galvanized and of different sizes so they had to be de-galvanized and custom fittings had to be engineered and fabricated for each wire. During de-galvanizing the labels on the wires where lost, so in order to determine the grade of the steel, a tensile strength test was performed. Dimensions, material properties and the results from the tensile strength test are listed in table 1. The fittings were made of 10mm round bar of magnetic steel, either turned on a lathe or trimmed to the required size with a steel mill. Figure 6 shows the four armour samples fitted with their custom steel adapters.

Sample no.	Height [mm]	Width [mm]	Diameter [mm]	Density [g/cm^3]	Tensile strength [N/mm^2]	Grade
1	7.400	2.350		7.8	792	65
2	9.250	2.800		7.8	372	34
3	8.900	3.400		7.8	667	65
4 (Round)			5.6	7.8	371	34

Table 1: Material properties and physical dimensions for the steel armour wires. Results from the tensile strength test with the resulting steel grade

(a) Sample no. 1: 7.400 × 2.350 mm

(b) Sample no. 2: 9.250 × 2.800 mm

(c) Sample no. 3: 8.900 × 3.400 mm

(d) Sample no. 4: 5.6 mm

Figure 6: Armour wire samples

3.1.3 Measuring procedure

The armour wire samples are exposed to both AC- and DC fields of different strengths in predefined sequences. The DC field measurement produces a new-curve from which the permeability can be determined. In addition to the permeability at different field strengths, the AC measurement also takes hysteresis into account. Based on this data, the software calculates different parameters that it uses to plot various quantities, such as power loss and differential permeability as functions of magnetic flux density. The following measurements are conducted for each of the four samples:

1. DC measurements:
   (a) Maximum field strength: $\vec{H} = 250\text{A/m}$
   (b) Maximum field strength: $\vec{H} = 1\text{kA/m}$
   (c) Maximum field strength: $\vec{H} = 5\text{kA/m}$
2. AC measurements at 50Hz:
   (a) Magnetizing sequence, $\vec{J}$-sequence: 1 mT to 100 mT in steps of 5 mT
   (b) Magnetizing sequence, $\vec{J}$-sequence: 100 mT to 2 T in steps of 100 mT

3.1.4 Results

The samples are tested according to the procedure and at the values listed in section 3.1.3. The New-curves from the DC measurement with a magnetic field strength of 5kA are displayed in figure 7 and 8. Two of the samples experience a higher flux density before they become saturated and will thus have i larger maximum permeability in the region before saturation. This is however in a region of the magnetic field $\vec{H}$, that is much greater then the armour wires will ever experience under normal operation and during the tests that are performed in section 3.6. Possible reasons for the variation will be briefly discussed in section 5.

For cable applications related to this thesis, the permeability for the armour wires must be determined from the expected magnetic flux density within the wires, produced by the magnetic filed from the conductors. From section 4.5, values of $\vec{B}$ in the armour wires never exceed 9mT with a relative armour permeability of 300. Figures 9 and 10 shows the power loss curves for the samples up to a magnetizing value of 2T. Figure 11 shows the new-curve up to 250A/m for sample no. 1, the same armour that is used for the cable in section 3.6.

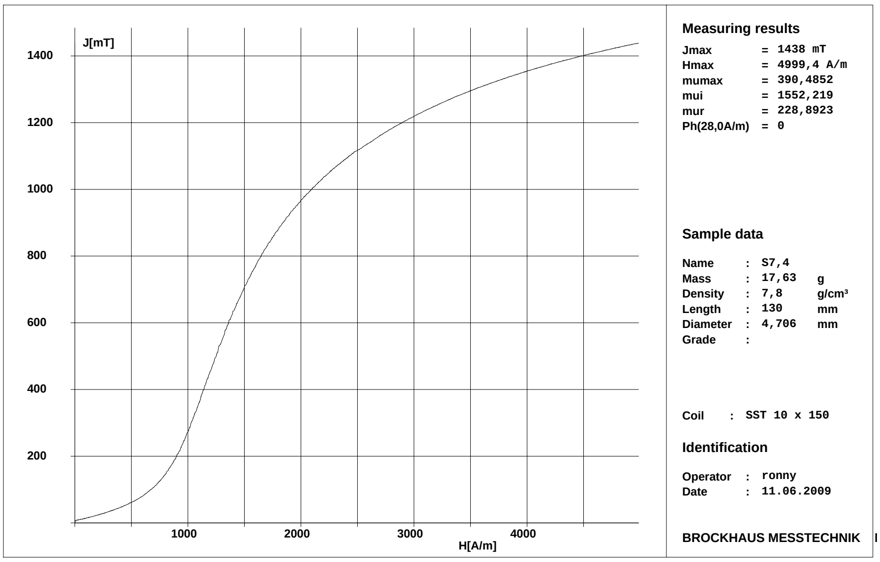

(a) Sample no.1

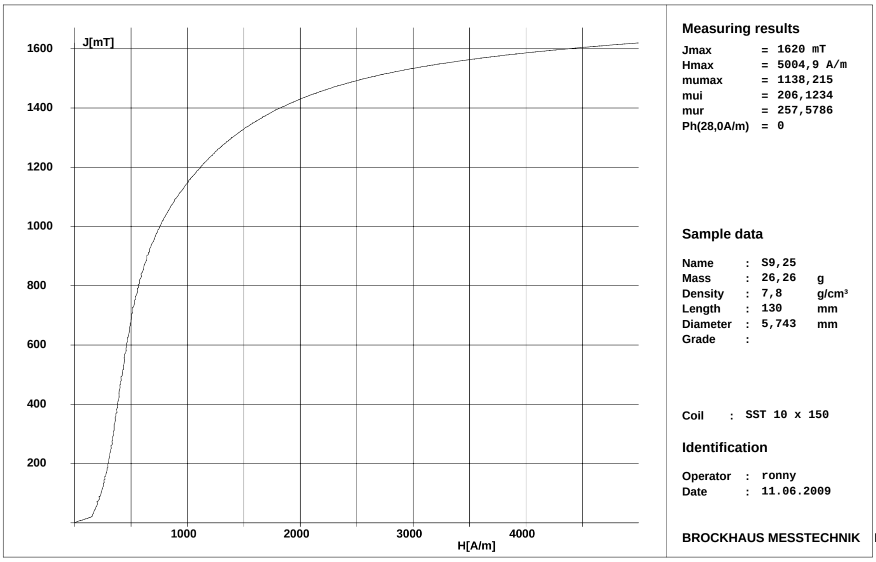

(b) Sample no.2

Figure 7: New curves up to 5 kA/m for samples 1 and 2

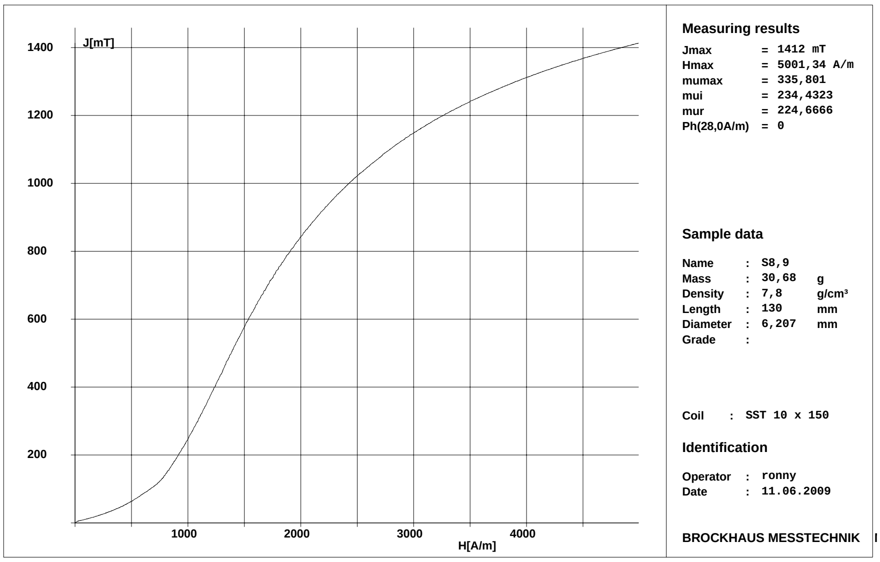

(a) Sample no.3

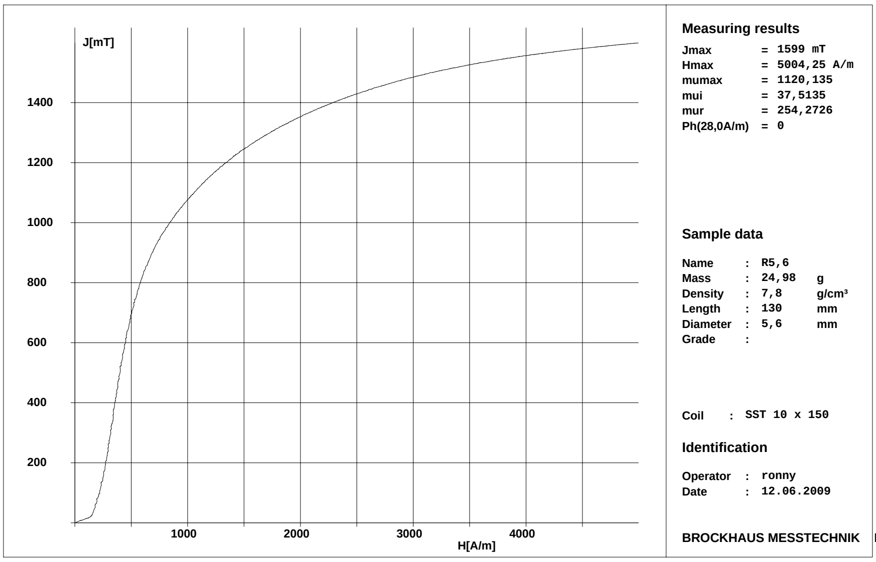

(b) Sample no.4

Figure 8: New curves up to 5 kA/m for samples 3 and 4

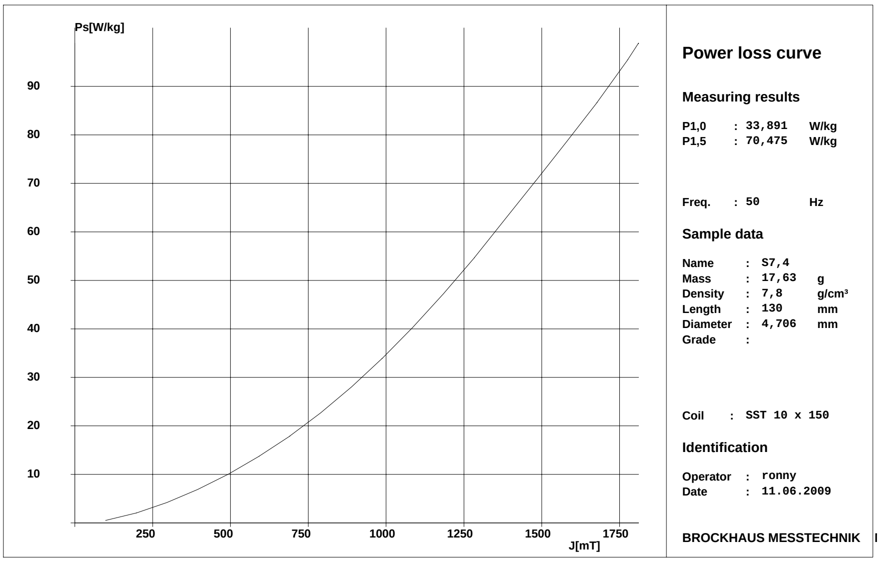

(a) Sample no. 1

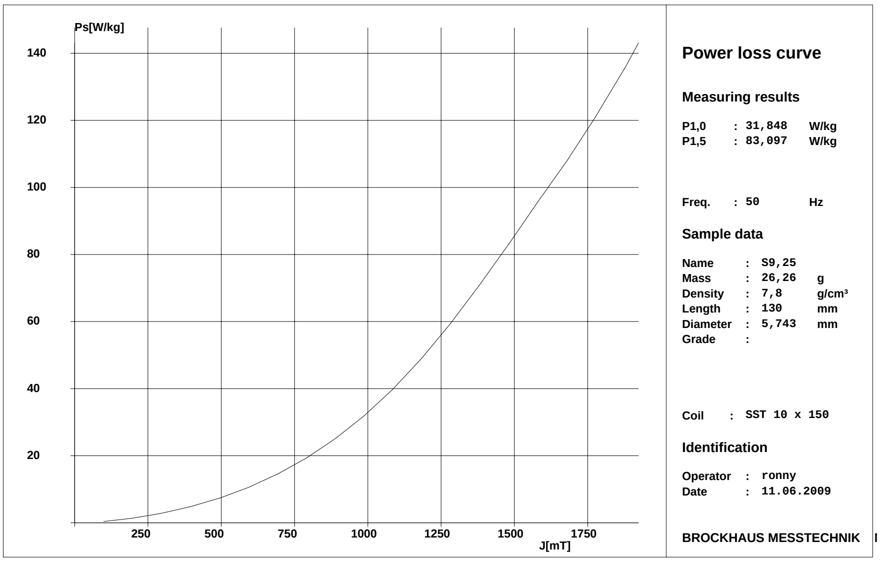

(b) Sample no. 2

Figure 9: Power loss curves for sample 1 and 2

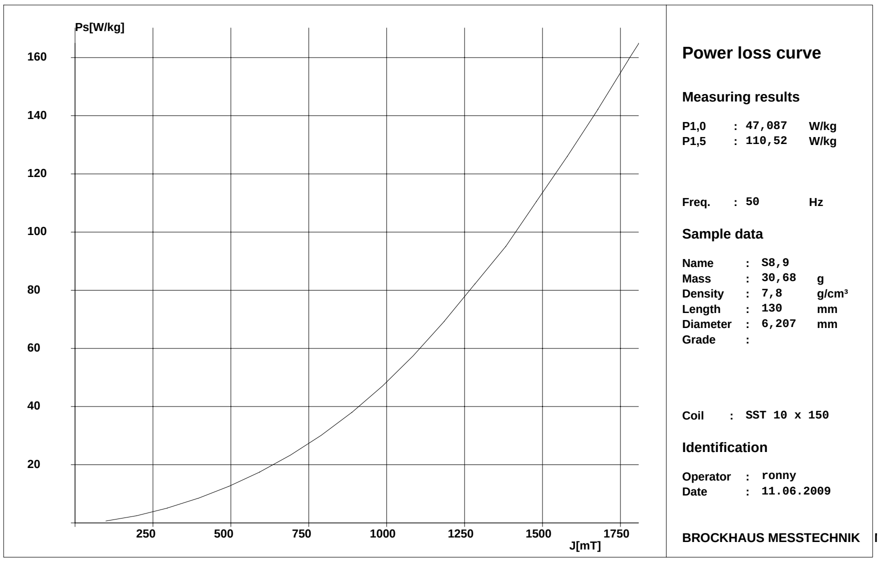

(a) Sample no. 3

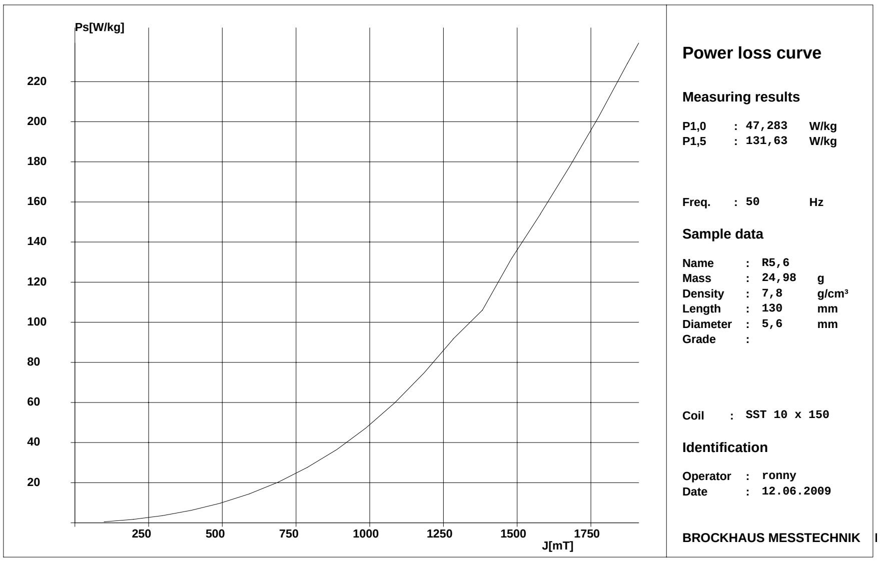

(b) Sample no. 4

Figure 10: Power loss curves for sample 3 and 4

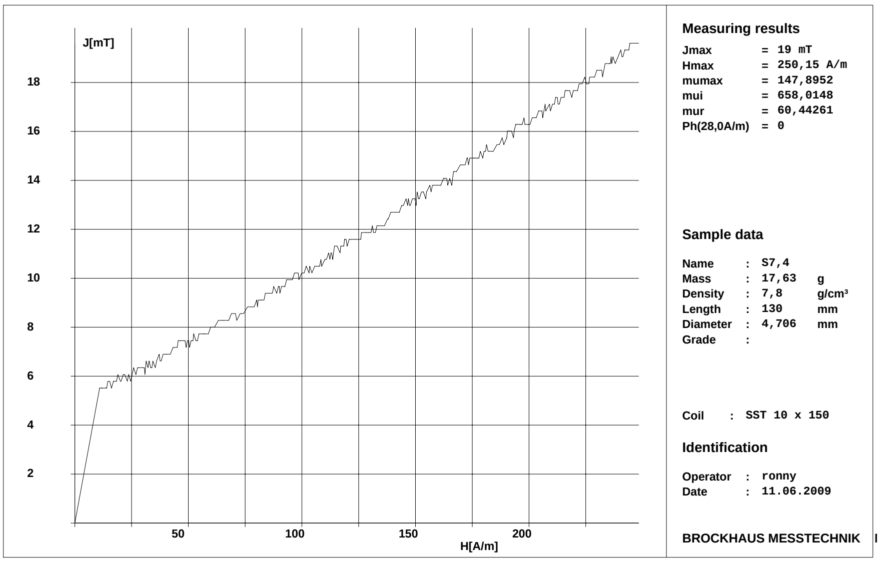

Figure 11: New-curve for sample no. 1 up to a field strength of 250A/m

3.2 Induced Loss in Cable Armour at Power Frequencies

To determine the amount of loss due to circulation currents in the armour , a small scale test is conducted in the laboratories at Nexans. If circulating currents in the armour account for a considerable amount of the total loss, a scaled down test consisting of a three-phase circuit inside metal armor of the types illustrated by figure 12 will provide evidence of this.

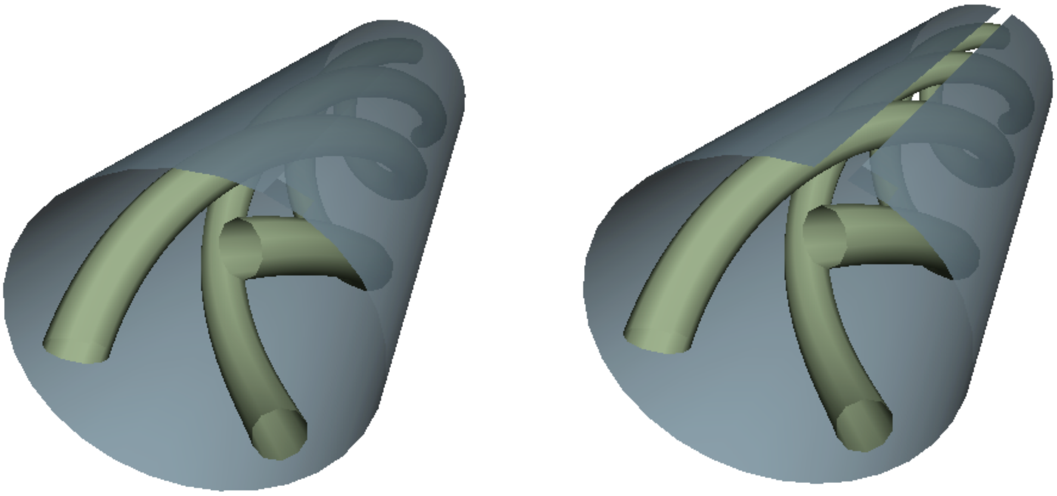

(a) Conductors inside intact metal pipe (b) Conductors inside split metal pipe

Figure 12: Illustration of conductors inside pipes

3.2.1 Test object

The set-up consists of a three-phase circuit of twisted 2.5 mm^2 conductors as shown in figure 13. Steel and copper pipes are used as armour. Details are listed below:

- Three-phase circuit:

  2.5 mm^2 copper conductors with length: $l_c = 5$m. Conductors are twisted around each other.

- Steel Armour:

  Length: $l = 2$m, Outer diameter: $d_o = 3/4"$, Thickness: $d_{thick} \approx 1$mm

  1. Intact pipe
  2. Split pipe

- Copper Armour:

Length: $l = 2$m, Outer diameter: $d_o = 3/4"$, Thickness: $d_{thick} \approx 1$mm

1. Intact pipe
2. Split pipe

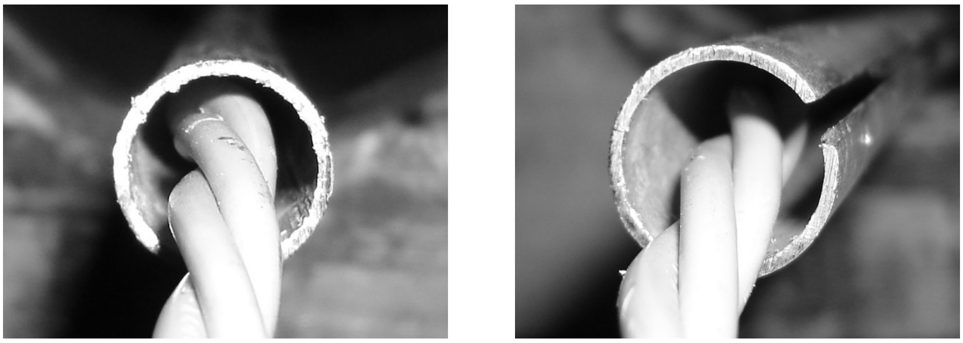

(a) Intact pipe (b) Split

Figure 13: Steel pipes with three twisted conductors inside

3.2.2 Equipment

The equipment used during the test is listed below:

- Variable auto transformer (Schuntermann)
- Frequency converter (Stadt Sinus)
- Wye connected load: $R_{phase} \approx 30\Omega$, $I_N = 7,5$A, $U_N = 400$V
- Temperature logger
- Hand held clamp-on instrument

3.2.3 Measuring procedure

The following three tests are conducted:

1. Conductors connected to additional load with variac as power source
2. Conductors short circuited with variac as power source
3. Conductors connected to additional load with frequency converter as power source

The test object is connected to the variable auto transformer and load as illustrated in the circuit diagram of figure 14. The voltage is increased until the load's nominal current is reached. For the second test, the load is disconnected and conductors short circuited. The voltage is increased until the current equals 30A. With a frequency of 120 Hz, provided by the frequency converter listed in section 3.2.2, the load is again connected for the third test. The converters output current limit is set equal to the load's current rating.

The temperature is, for all the cases listed above, captured with a temperature sensor and logged by the printer.

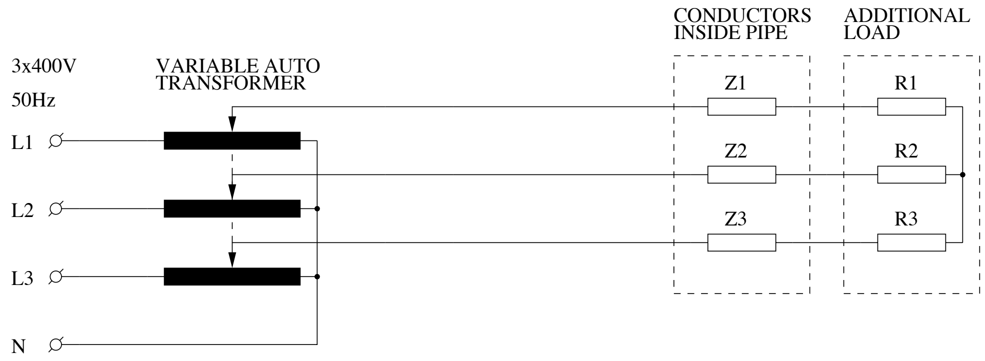

Figure 14: Circuit diagram for experimental test of induced circulating currents at 50 Hz with load connected

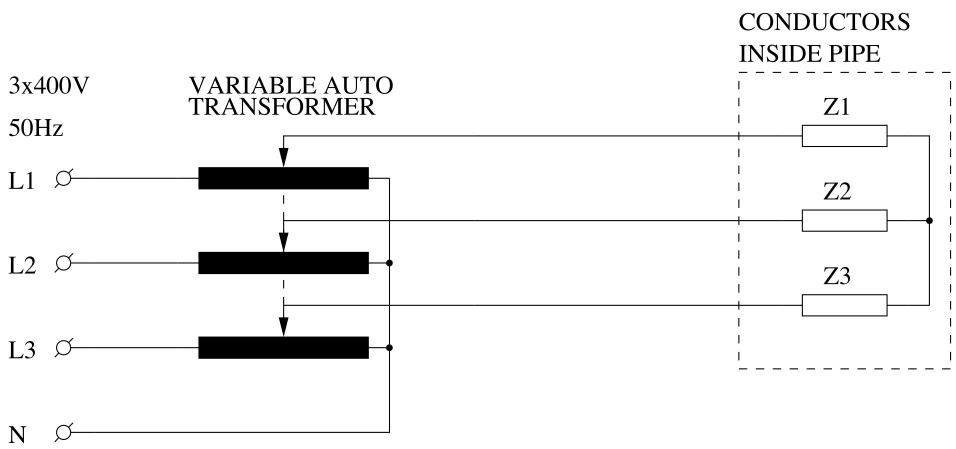

Figure 15: Circuit diagram for experimental test of induced circulating currents at 50 Hz with no load connected

3.2.4 Results

The first test provided no immediate increase of the pipes surface temperature. To be able to tell if the temperature increase is due to induced currents exclusively, the temperature

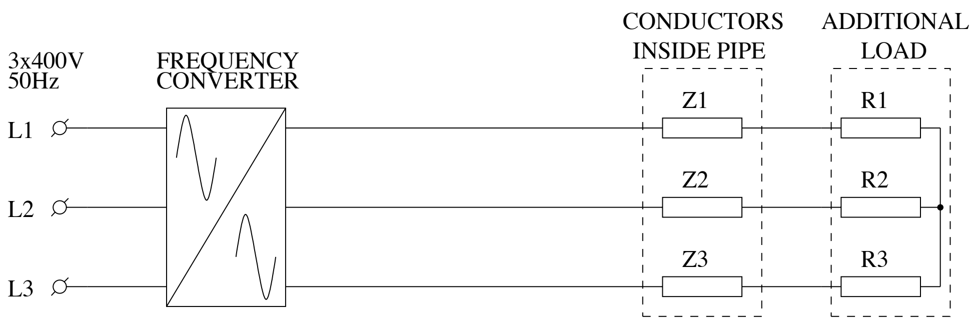

Figure 16: Circuit diagram for experimental test of induced circulating currents at 120 Hz with load connected

has to increase significantly over period of time before the heat from the conductors contribute to the measured temperature. The measured temperature for intact copper and steel pipes is shown in figure 17. The results from the second and third test is shown in figures 18 and 19 respectively. Of the two final tests, the second had the steepest increase with approximately 1°C/min. Increasing the frequency to 120 Hz did not contribute to significantly steeper increase of temperature compared with 50 Hz.

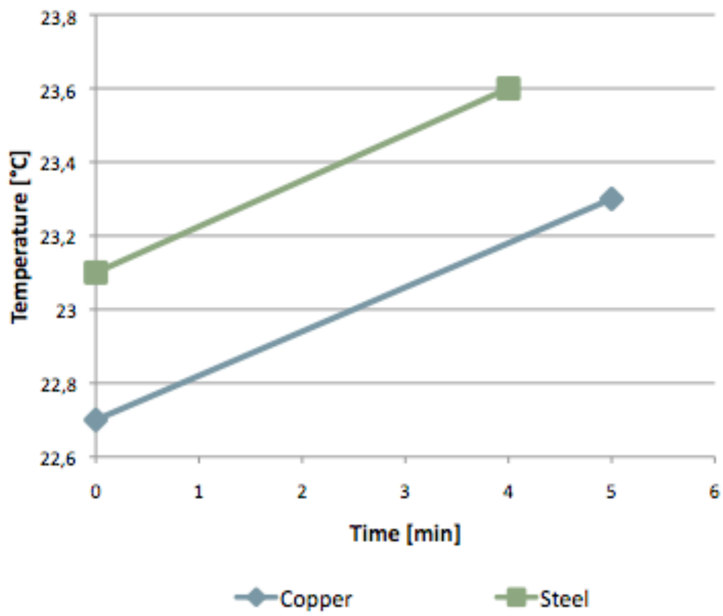

Figure 17: Temperature increase in intact copper and steel pipe at 50 Hz and 7.5A

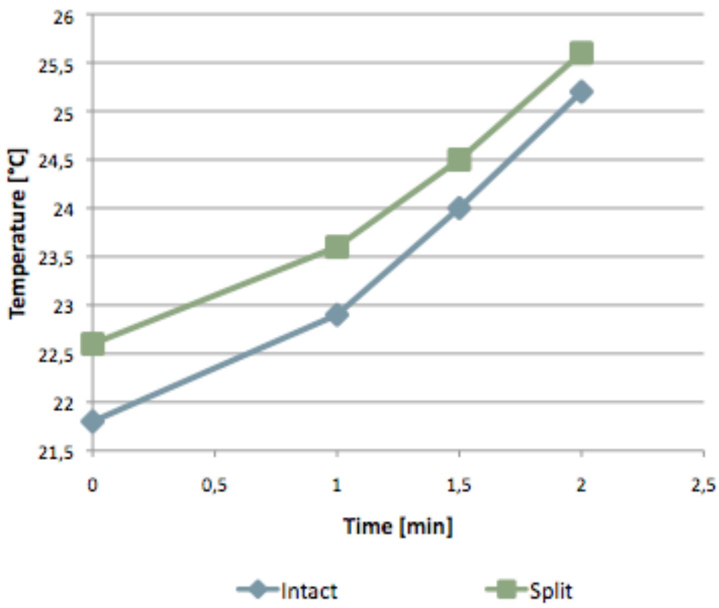

Figure 18: Temperature increase in split and intact steel pipe at 50Hz and 30A

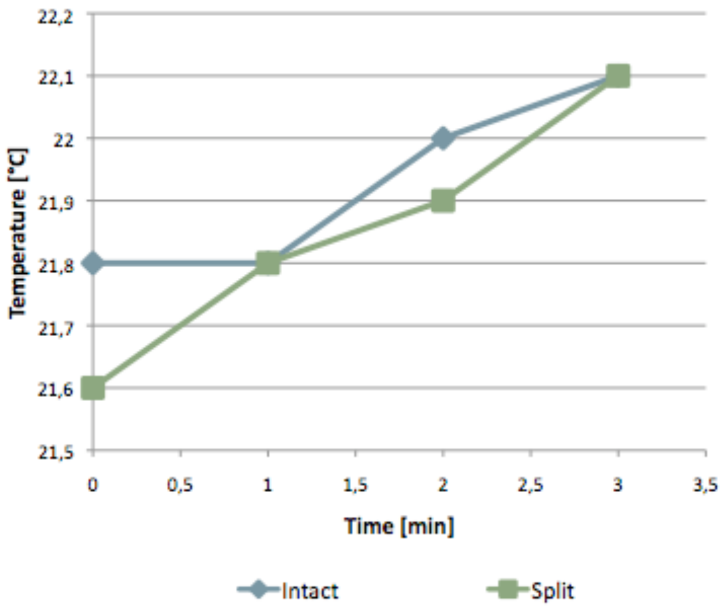

Figure 19: Temperature increase in split and intact steel pipe at 120Hz and 7.5A

3.3 Induced Loss in Cable Armour at High Frequencies

With no apparent loss due to circulating currents at typical power frequencies, a higher ranging frequency converter is used in a second attempt in the laboratories at NTNU. The highest rated converter available is a 20kW electric drive converter with internal logic, designed for use with digital signal processors. Computer simulations prior to testing revealed that the rated values would be sufficient to induce losses that could easily be detected by thermal sensors.

3.3.1 Test object

Two three-phase circuits are constructed. Each circuit consists of three 35 mm^2 copper conductors that are mounted 120° apart on a 10 mm diameter plastic spacer. Steel and copper pipes are used as armour by placing one of the circuits inside. Details are listed below:

- Three-phase circuits:

  35 mm^2 copper conductors with length: $l_c = 2.7$m. Spacer diameter and lenght: $d_s = 10$mm, $l_s = 2$m. Centre to centre distance of spacer and conductors: $r_{c-c} \approx 8,8$mm. Conductors are short circuited in one end.

  1. Conductors parallel to spacer
  2. Conductors twisted sex times around the spacer over the entire length

- Steel Armour:

  Length: $l = 2$m, Outer diameter: $d_o = 35$mm, Thickness: 1.5mm

  1. Intact pipe
  2. Split pipe

- Copper Armour:

  Length: $l = 2$m, Outer diameter: $d_o = 36$mm, Thickness: 2mm

  1. Intact pipe
  2. Split pipe

3.3.2 Equipment

The converter has a current limit of 50A at 10kHz. Initial attempts to program a DSP to use as controller for the converter proved too time consuming, and was aborted in favor of LabVIEW virtual instruments. A brief description of the program is found in section 3.3.3. The converter is fed with a dc-link from a rectifier. The converters output power is controlled by limiting the voltage input of the rectifier with a variable auto transformer. Figure 20 shows the circuit diagram for the test. Five thermal sensors are connected to a computer logger and measure the temperature on both ends and the centre of the pipes surface, on the surface of the conductors and the ambient air. An oscilloscope is used to measure the conductors phase-voltage and current. In addition to the thermal sensors, a thermal imaging camera is used to capture the temperature on the surface of the pipes. The camera is calibrated and placed to capture the temperature next to the middle thermal sensor. Figure 21 shows photos taken of the set-up in the laboratory.

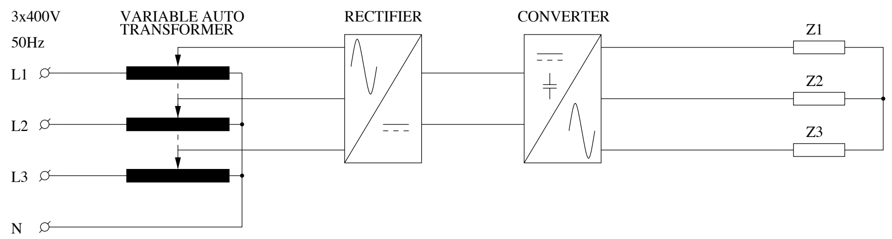

Figure 20: Circuit diagram for induced loss at high frequency

3.3.3 Converter controller design

The converters logic circuit is displayed in figure 22. The converter is a three-leg full bridge thyristor converter. Its internal logic allows for the construction of a simple controller. When A+ is "1", A- is automatically shifted to "0" by the negated input from A+ on the AND-port. As a consequence, both thyristors on any leg, can never by turned on simultaneously. Additionally every thyristor has its own time delay to further reduce the risk of short circuit on a leg. Setting A-, B- and C- constantly equal to "1", only three signals (A+, B+ and C+) need to be controlled. The inputs are turned high every 360°, or every $1/f$ seconds, and remain high for a duration of $1/(2f)$ seconds. Each signal is phase-shifted 120°, or $1/(3f)$ seconds. Choice of frequencies are based on the derived time delays in order to achieve a symmetrical three-phase converter output, see equation (3) and (4). The virtual instrument diagram is shown in appendix B.1.

$$t = \frac{1}{f} = \frac{1}{8333.33} = 12 \cdot 10^{-5}[\mathrm{s}] \tag{3}$$

$$t_{delay} = \frac{t}{3} = \frac{12 \cdot 10^{-5}}{3} = 4 \cdot 10^{-5}\,[\mathrm{s}] \tag{4}$$

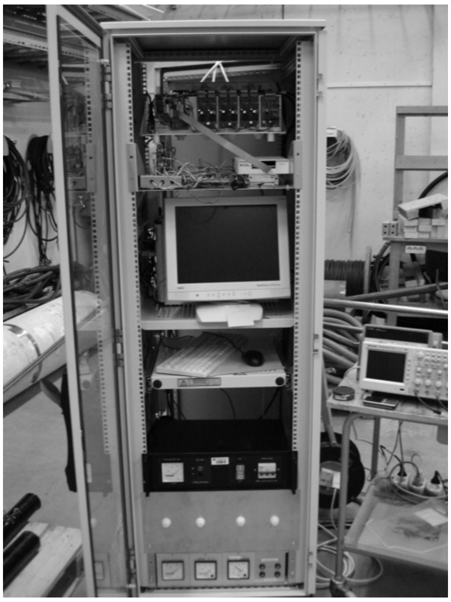

(a)

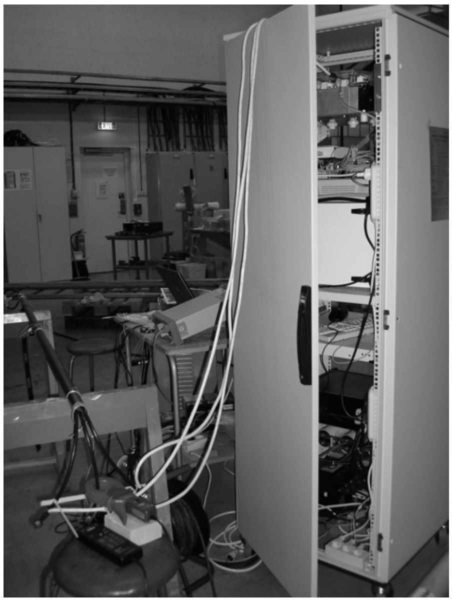

(b)

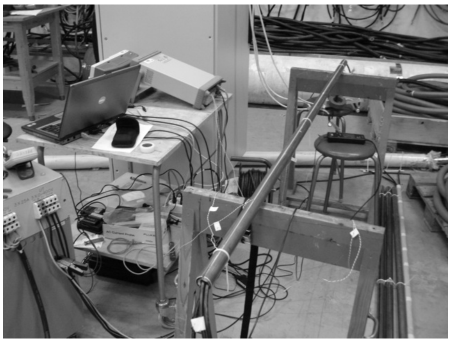

(c)

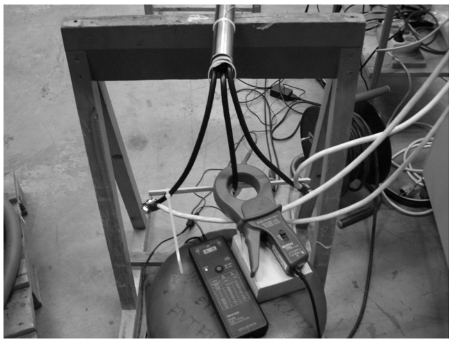

(d)

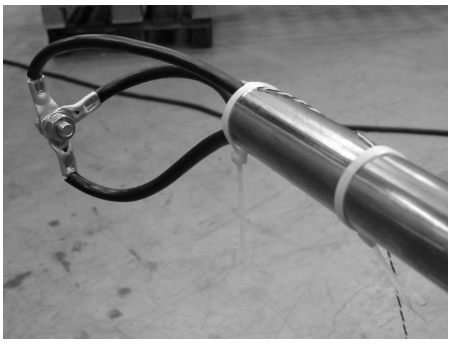

(e)

(f)

Figure 21: Pictures from laboratory test: (a): front of the cabinet housing converter, rectifier and controller. (b): connections from the load to the converter. (c): variac, test object, loggers. (d): voltage probe and current clamp. (e): wye-point of conductors. (f): temperature sensor

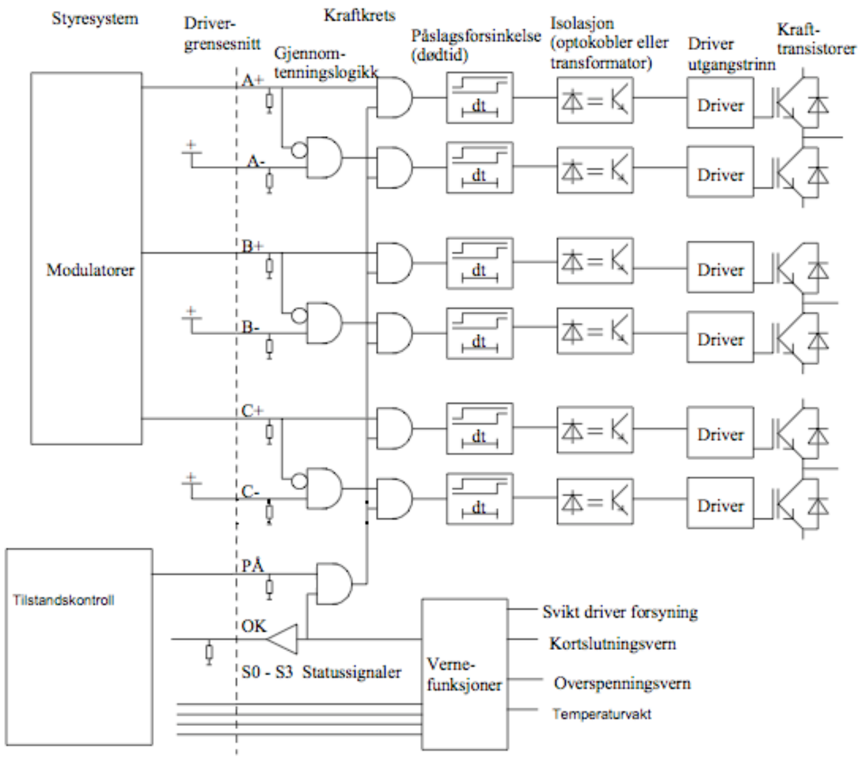

Figure 22: Circuit diagram for the converter logic

3.3.4 Measuring procedure

The converter is turned on and the output current is increased by increasing the voltage output from the variac up to its current limit of $I_{v,max} = 25$A, measured with a current clamp connected to a voltmeter. Current and voltage plots are captured at $I_{v,max}$. Temperature is captured continuously every 1 second. Thermal images from the camera are captured manually. This procedure is repeated for every armor, resulting in a total of four tests.

3.3.5 Results

The experiment is conducted as described in section 3.3.4. Initial tests proved no difference between parallel and twisted conductors inside the intact pipes. For this reason, the parallel conductors are omitted from further study. Figure 23 shows the current and phase voltage plot for twisted conductors with intact copper pipe. The oscilloscope did not respond well to these high frequency signals, all though scope and both probes were rated to handle higher frequencies then this. Without the correct RMS values of current and voltage, the temperature data is the only possible option for calculating the loss. The thermal images of figure 24, provide a visible illustration of the increase of temperature during the test of the intact steel pipe with twisted conductors. They provide no practical advantage over the temperature sensors, unless the data is captured continuously in real time. Figures 25 and 26 show the plots of temperature increase for both intact and split, copper and steel pipes, respectively.

Temperature increase for intact and split pipes are compared for both copper and steel in figure 27. Using equations (1) and (2) from section 2.4, the total resistive loss for each pipe is calculated. ΔT is determined in a linear region the first few seconds after power-on, where the heat from the conductors do not contribute to the temperature on the pipe surface. Equations (5) and (6) shows the calculation for the intact copper pipe. The rest of the results are listed in table 2.

$$\Delta W = C_{P_{Cu}}\, m_{Cu_{Intact}}\, \Delta T = 0.39\,[k\mathrm{J}\, k\mathrm{g}^{-1}\, \mathrm{K}^{-1}]\, 2.725\,[k\mathrm{g}]\, 0.2\,[\mathrm{K}] = 0.21255\,[k\mathrm{J}] \tag{5}$$

$$P = \frac{\Delta W}{\Delta t} = \frac{0.21255\,[k\mathrm{J}]}{30\,[\mathrm{s}]} = 7.1\,[\mathrm{W}] \tag{6}$$

Material	Description	C_P [kJ kg^{-1} K^{-1}]	m [kg]	ΔT [°K]	Δt [sec]	P [W]
Copper	Intact	0.39	2.725	0.2	30	7.1
	Split	0.39	2.655	0.2	30	6.9
Steel	Intact	0.49	2.290	0.4	6	74.8
	Split	0.49	2.235	0.4	6	73.0

Table 2: Calculated loss and material properties (Specific heat capacity C_P, mass of pipes m and temperature and time, in degrees Kelvin and seconds respectively).

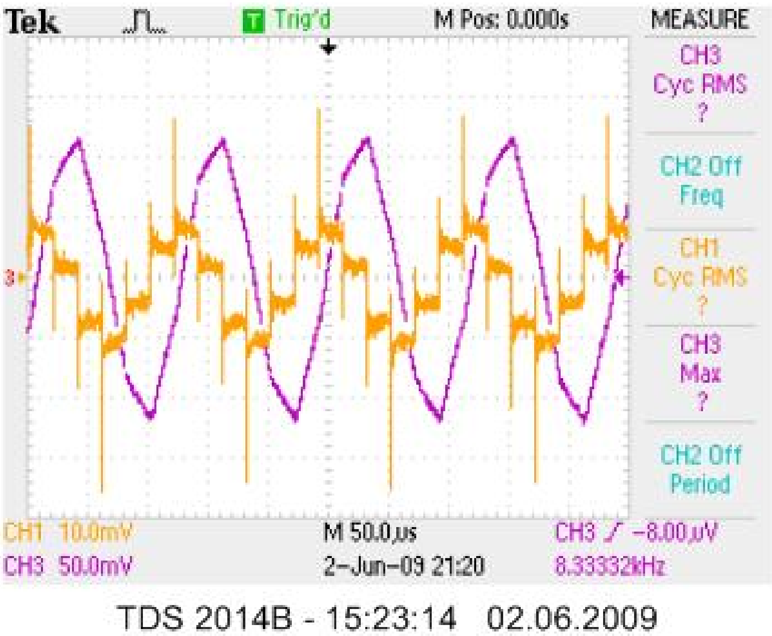

Figure 23: Phase voltage and current for intact copper pipe with twisted conductors

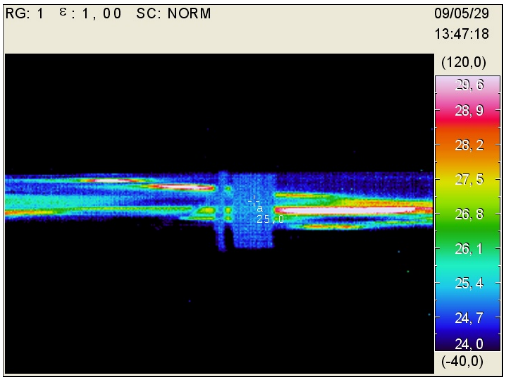

(a) 25°C at $t = 0$s

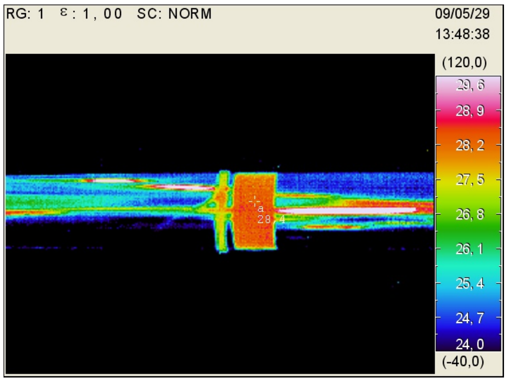

(b) 28.4°C at $t = 1:20$s

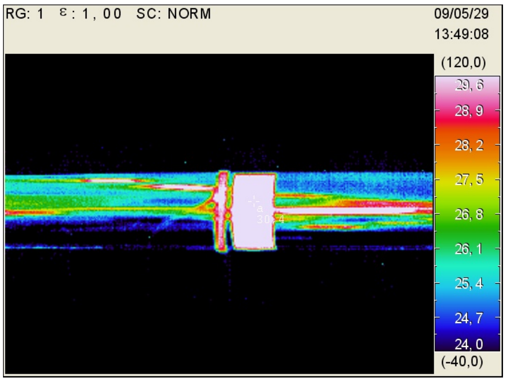

(c) 30.4°C at $t = 1:50$s

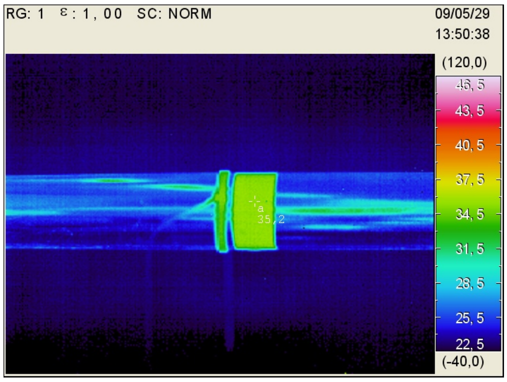

(d) 35.2°C at $t = 3:20$s

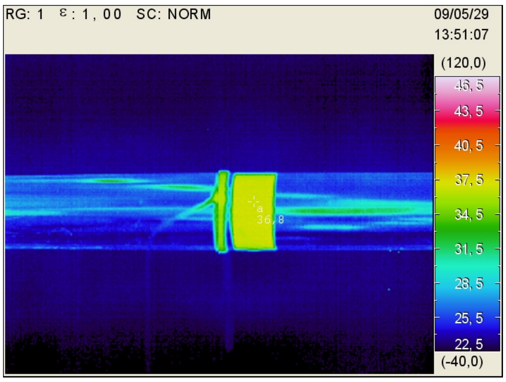

(e) 36.8°C at $t = 3:49$s

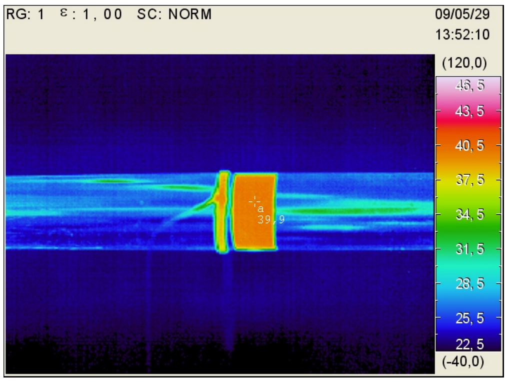

(f) 39.9°C at $t = 4:52$s

Figure 24: Thermal images captured during test of split steel pipe. The range is adjusted after image (c).

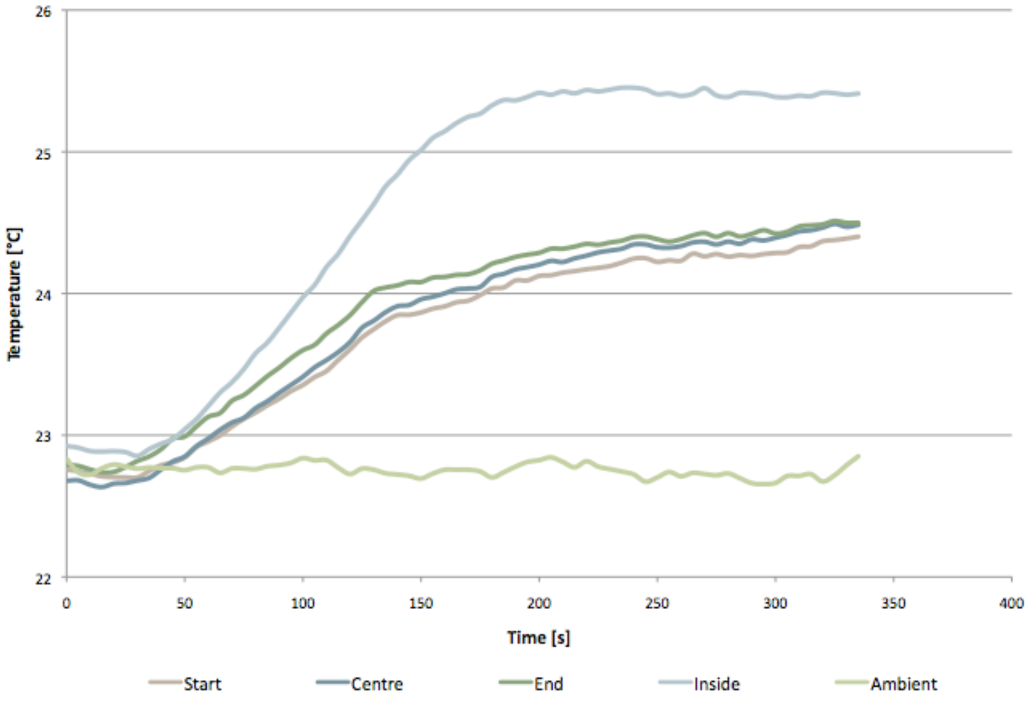

(a) Temperature increase of intact copper pipe

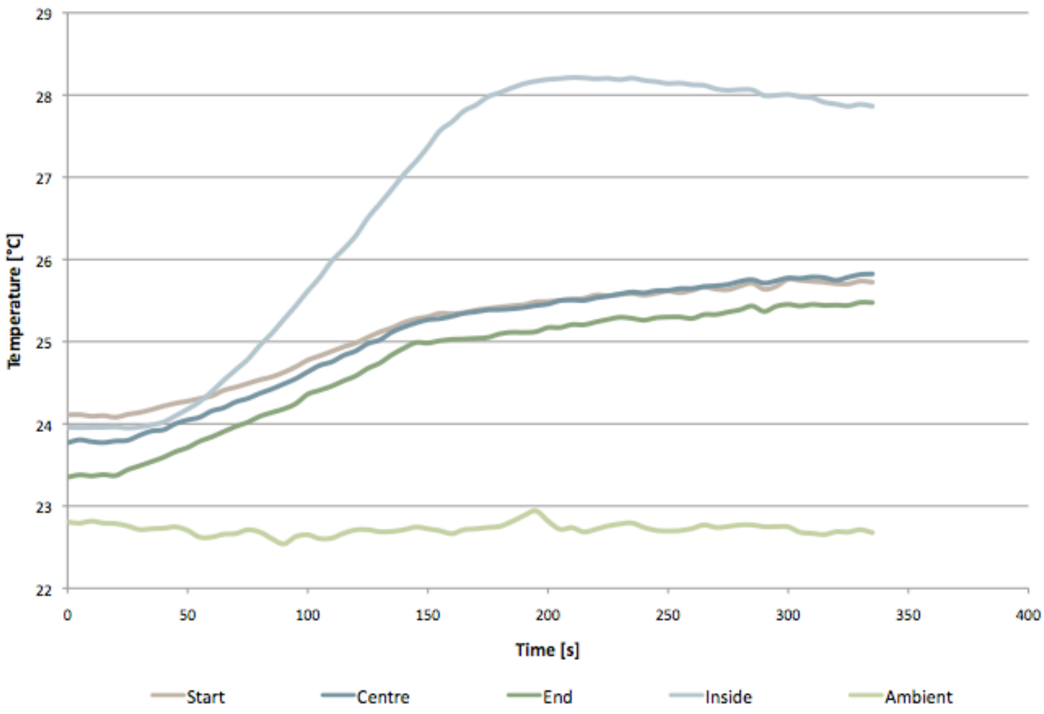

(b) Temperature increase of split copper pipe

Figure 25: Temperature increase in °C of pipes due to induction currents in (25a) intact copper pipe and (25b) split copper pipe.

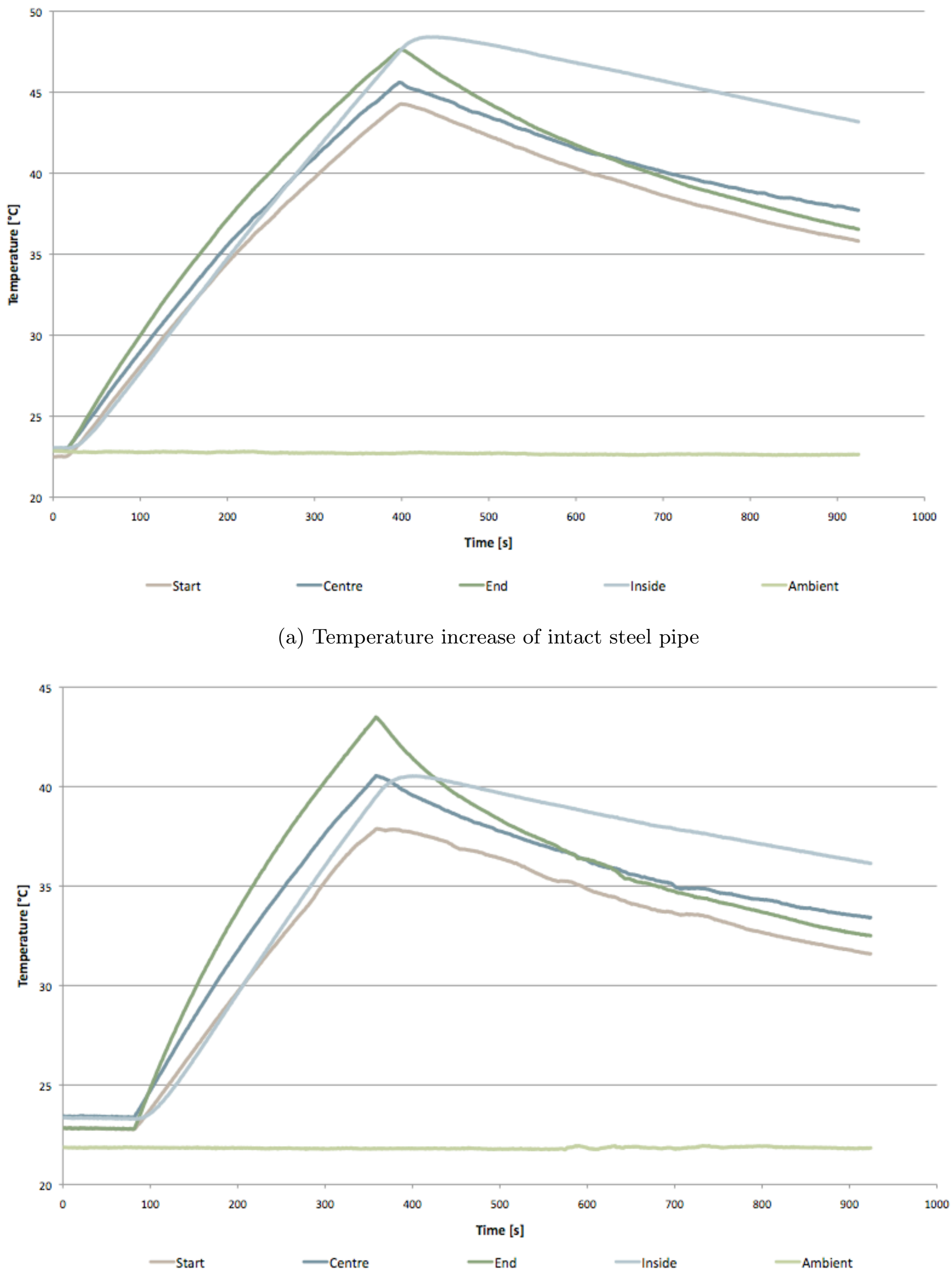

(a) Temperature increase of intact steel pipe

(b) Temperature increase of split steel pipe

Figure 26: Temperature increase in °C of pipes due to induction currents in (26a) intact steel pipe and (26b) split steel pipe.

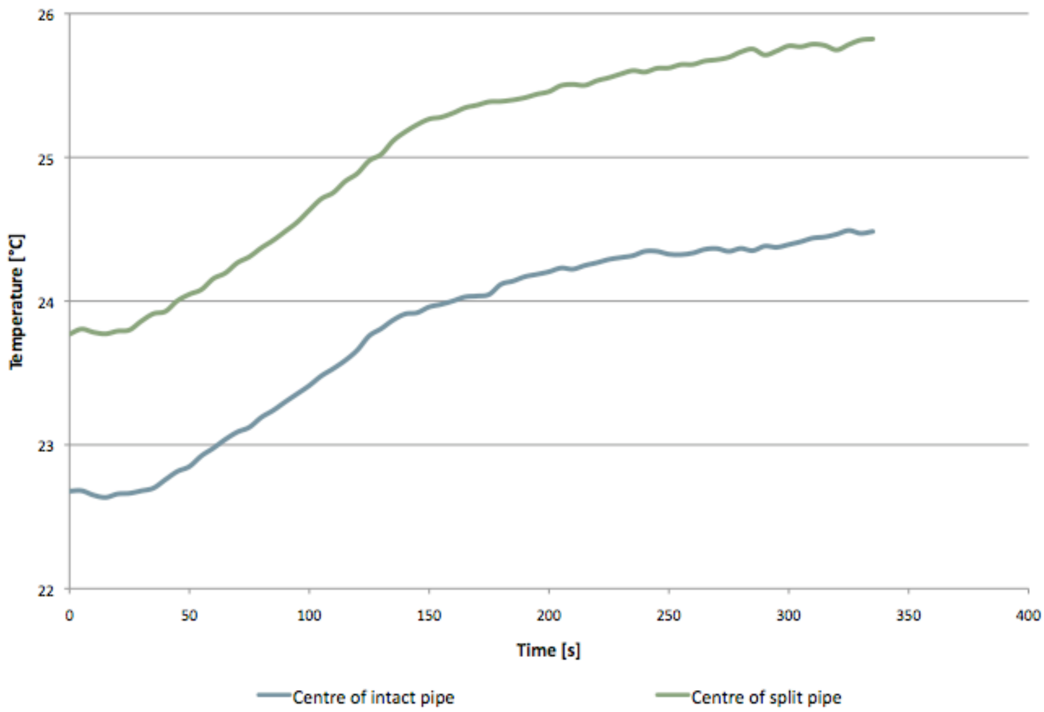

(a) Intact and split copper pipe

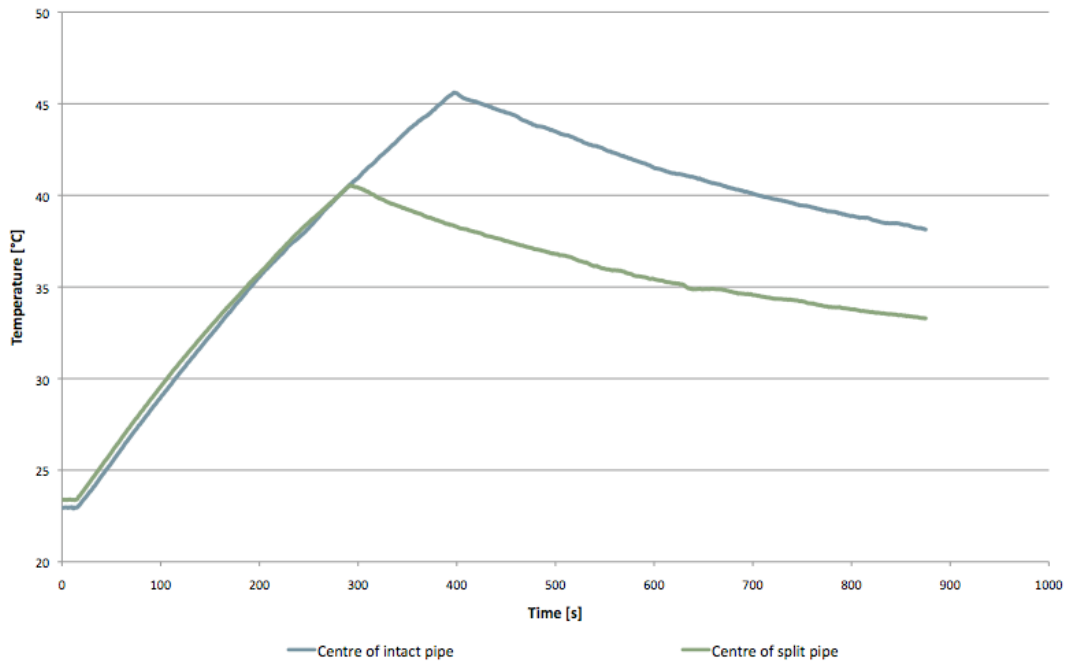

(b) Intact and split steel pipe

Figure 27: Comparison of temperature increase for split and intact pipes. (a): Copper pipe. (b): Steel pipe

3.4 Induced Voltage in Parallel Conductors

In order to prove the theory described in section 2.1, a laboratory test consisting of a three phase circuit and an open measuring loop is constructed.

3.4.1 Test object

The set-up is pictured in figure 28. The loop consists of 0.5 mm^2 copper conductor with a total length of 4 meters. The distance between the conductors that make up the measuring loop is 5 cm. The reason for constructing the measuring conductor as a loop and twisting the ends is to avoid induced voltage[1] in parts of the measuring circuit that is not suppose to be active. The same conductor circuits constructed for the tests of section 3.3 are used:

- Three-phase circuits:

  35 mm^2 copper conductors with length: $l_c = 2.7$m. Spacer diameter and lenght: $d_s = 10$mm, $l_s = 2$m. Centre to centre distance of spacer and conductors: $r_{c-c} \approx 8,8$mm. Conductors are short circuited in one end.

  1. Conductors parallel to spacer
  2. Conductors twisted sex times around the spacer over the entire length

- Measuring loop

  0.5mm^2 copper conductor. Active induction length: 4m. Geometric mean distance between path and return path: $d_{c-c} = 5$ cm

3.4.2 Equipment

The frequency converter from section 3.3.3 is used. An oscilloscope with a higher sampling frequency (1.25 GS/s) is connected to the ends of the loop. The converter is connected to the three-phase circuit.

3.4.3 Measuring procedure

The converter is first connected to the parallel circuit. The converter is turned on and the voltage from the variac is increased until the current output from the variac reaches 25 A. The induced voltage in the loop is captured on the oscilloscope. The same procedure is repeated with the twisted circuit connected to the converter.

[1]though not yet documented in this thesis.

(a) Return point of measuring loop

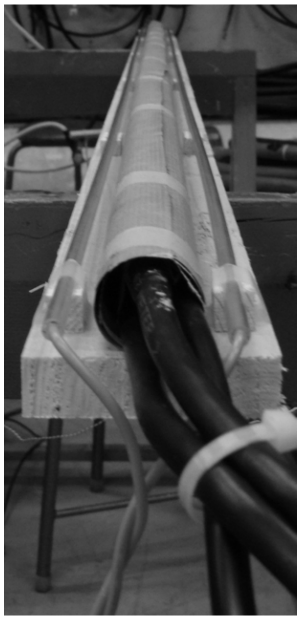

(b) Terminal of loop

Figure 28: Test set-up for induced voltage in parallel conductors

3.4.4 Results

Following the procedure of section 3.4.3, the induced voltage for both conductor arrangements is captured and displayed in figure 29. The induced voltage of figure 29b is almost completely canceled when the conductors are twisted.

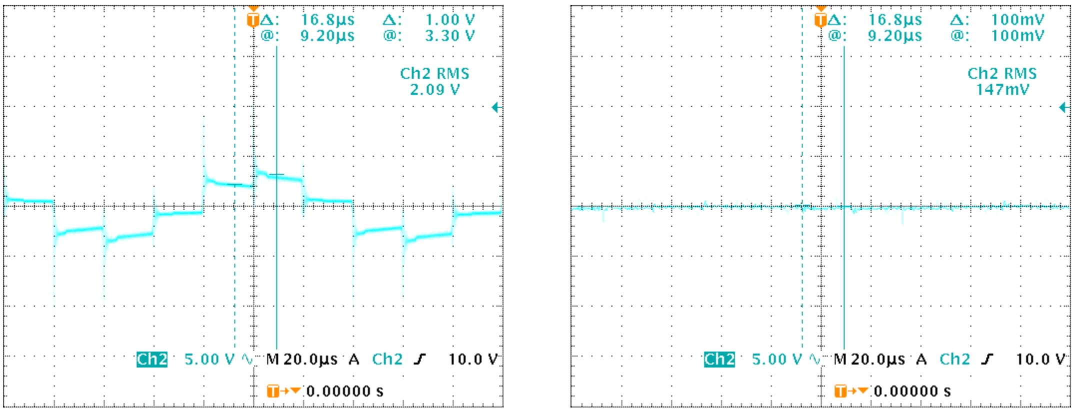

(a) Induced voltage with parallel conductors (b) Induced voltage with twisted conductors

Figure 29: Induced voltage in measuring loop with: (a) parallel conductors and (b) twisted conducters

3.5 Measurements on Power Cable

Figure 30: TKRA 245 kV $3 \times 1 \times 500\text{mm}^2$ KQ + FO

The measurements on TKRA 245 kV $3 \times 1 \times 500\text{mm}^2$ KQ + FO displayed in figure 30 are conducted during the summer on Nexans factory in Halden.

3.5.1 Test object

The cross section TKRA 245 kV $3 \times 1 \times 500\text{mm}^2$ KQ + FO is illustrated in figure 31. The constituents of the cable are listed in table 3. Cable length is approximately 8.4 km.

3.5.2 Equipment

The equipment used during the test is listed below:

- Variable auto transformer (Schuntermann)
- Three voltage measurement transformers.
- Precision power meter LMG 500
- Hand held clamp-on instrument

3.5.3 Measuring procedure

The equipment and cable are connected according to figure 32. The cables phases are directly connected to the variac in one end and short circuited on the other end. The screens are short circuited in both ends, allowing induced currents to flow freely (see figure 33a and 33c). The armour wires are short circuited in both ends and connected together with a copper conductor. Individual wires are bent up, as pictured in figures 33b,

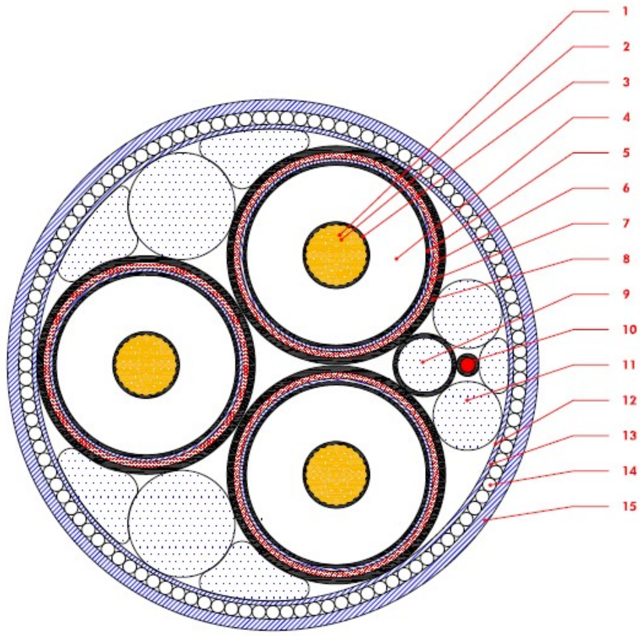

Figure 31: Cross section of TKRA 245 kV 3x1x500 mm2 KQ + FO

No.	*Constituents*	*Thickness* [mm]	*Diameter* [mm]
1	Conductor, stranded copper wires	61 × ∅3.30	26.5
2	Semiconducting filling compound		
3	Semiconducting XLPE		
4	Insulation, XLPE	25.0	79.5
5	Semiconducting XLPE		
6	Semiconducting swellable tape		
7	Lead sheath, alloy 1/2 C	2.7	
8	Sheath, semiconducting PE	2.6	96.5
9	Filler element with semiconducting sheath		
10	Fiber optic cable unit (36 fibers)		
11	Filler elements, PP		
12	Binder tape		
13	PP and bitumen		
14	Armour, galvanized steel wires	110 × ∅6.0	
15	PP and bitumen		235

Table 3: Constituents list for TKRA 245 kV 3x1x500 mm2 KQ + FO

in order to measure any currents that may flow in the armour The screens and armour wires are connected in one end to avoid any potential difference that may arise. To obtain an artificial neutral point, the three voltage transformers primary windings are connected in a wye-configuration. The wye neutral point of the windings is connected to the power meters voltage neutral connection pictured in figure 33d.

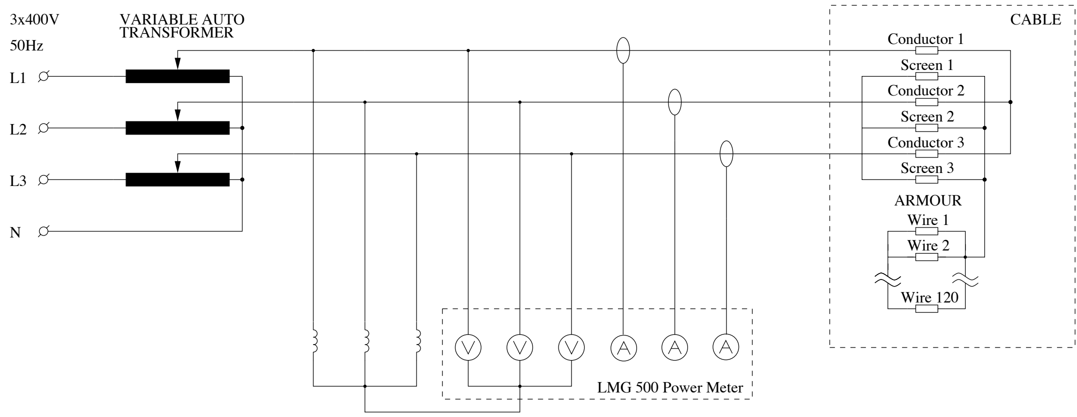

Figure 32: Circuit diagram for test conducted on power cable

3.5.4 Results

The measured values of phase voltage and current are listed in table 4. Measured active- and reactive power is listed in table 5. The screen currents have an average of 10A. The average resistance and -inductance are calculated in equations (7) and (8). The average ambient temperature for this time of year is, according to gathered weather data, approximately 20°C. Measured current in armour wires equal 0A.

$$R = \frac{P_{Avg}[\mathrm{W}]\,1000\,[\mathrm{m\,km^{-1}}]}{I_{Avg}^2[A]\,8400\,[\mathrm{m}]} = 0.0585\,[\Omega\,\mathrm{km^{-1}}] \tag{7}$$

$$L = \frac{Q_{Avg}[\mathrm{VAr}]\,1000\,[\mathrm{m\,km^{-1}}]}{\omega\,[s^{-1}]\,I_{Avg}^2[A]\,8400\,[\mathrm{m}]} = 0.466\,[\mathrm{mH\,km^{-1}}] \tag{8}$$

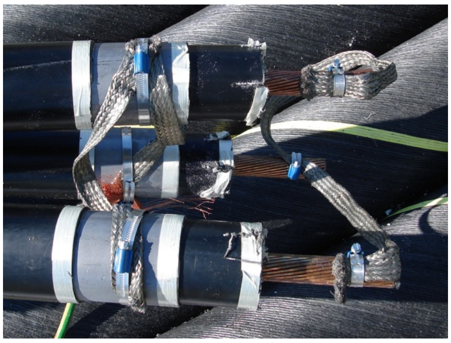

(a) Conductors and screens short circuited

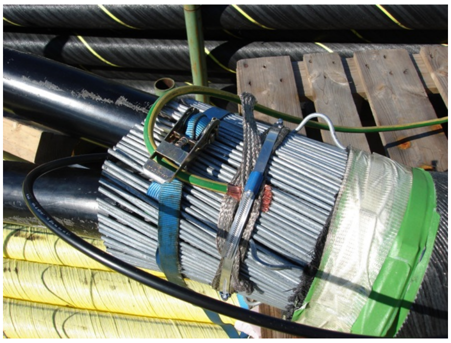

(b) Armour wires bent up for use of clamp-on instrument

(c) Overview of instrument connections

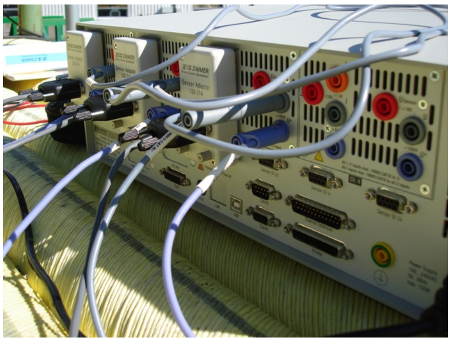

(d) Connections for power meter

Figure 33: Pictures from measurements of TKRA 245 kV 3x1x500 mm2 KQ + FO

	Conductor 1		Conductor 2		Conductor 3	
	Magnitude	Angle [°]	Magnitude	Angle [°]	Magnitude	Angle [°]
Voltage [V_{RMS}]	69.8	0.0	63.5	123.0	69.1	-114.0
Current [A_{RMS}]	50.948	-65.288	51.349	54.636	50.372	174.952

Table 4: Measured currents and voltages

	Conductor 1	Conductor 2	Conductor 3
Active Power [W]	1487	1202	1129
Reactive Power [VAr]	-3232	-3029	-3294

Table 5: Measured active- and reactive power

3.6 Measurements on Power Umbilical

Figure 34: TXVE 36 kV $6 \times 1 \times 95\,\mathrm{mm}^2$

The SRSWI (Sub sea Raw Sea Water Injection) power system is designed to feed two identical sub sea transformers with variable voltage and frequency, in order to individually operate two VSDs (Variable Speed Drives). The whole power cable system consists of four cable sections; a dynamic section from top side to the sea floor, a static section placed along the sea floor and two split-out sections – one to each transformer.

3.6.1 Test object

The measurements are carried out after the static- and dynamic sections are joined together. The total length of the two sections is 30 650 m. Figure 34 shows a picture of the cable the final day of measurements. The cable is tested both before- and after it is armoured. Figure 35 shows the cross section for the dynamic and static sections. The difference between the two sections in terms of magnetic parameters, are the dynamic section's steel ropes and two additional layers of armour.

3.6.2 Equipment

The equipment used during the test is listed below. Technical data for instruments and equipment is found in appendix A:

- Frequency converter (Stadt Sinus)
- Coupling transformer (Elinduktra)
- High voltage power transformers
- Three voltage measurement transformers.
- Precision power meter LMG 500

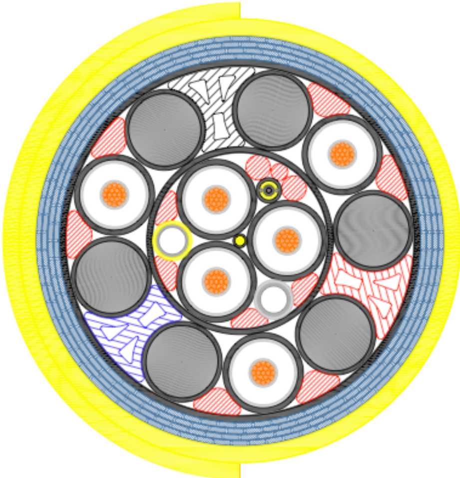

(a) Dynamic section

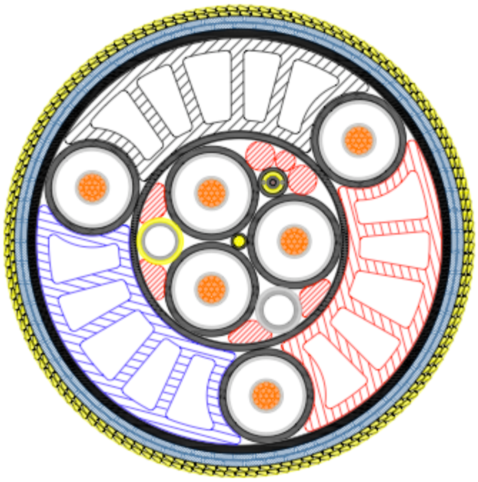

(b) Static section

Figure 35: Cross section of (a) dynamic- and (b) static section

- Hand held clamp-on instruments

3.6.3 Measuring procedure

The equipment is connected to the cable as illustrated in figure 36. The cable is tested at 20, 40, 50, 60, 70, 80, 100 and 120 Hz. Currents, phase voltages and their phase angles are measured for both inner- and outer circuit at all frequencies.

3.6.4 Results

All the values for currents, voltages and their phase angles would span several pages– as a consequence, only the calculated parameters are presented here. Tables 6 and 7 lists the calculated parameters for inner- and outer circuit on both armoured and unarmoured cable.

	Inner Circuit					
	Unarmoured			Armoured		
f [Hz]	Z_{ph} [$\Omega\,\mathrm{km}^{-1}$]	R_{ph} [$\Omega\,\mathrm{km}^{-1}$]	L_{ph} [$\mathrm{mH\,km}^{-1}$]	Z_{ph} [$\Omega\,\mathrm{km}^{-1}$]	R_{ph} [$\Omega\,\mathrm{km}^{-1}$]	L_{ph} [$\mathrm{mH\,km}^{-1}$]
20	0.184	0.178	0.400	0.184	0.178	0.389
40	0.208	0.177	0.438	0.207	0.177	0.425
50				0.223	0.177	0.434
60	0.242	0.176	0.446	0.242	0.177	0.436
70	0.263	0.176	0.448	0.262	0.177	0.439
80	0.285	0.176	0.450	0.283	0.177	0.440
100	0.332	0.175	0.452	0.329	0.176	0.443
120	0.382	0.173	0.454	0.379	0.175	0.446

Table 6: Calculated parameters for inner circuit for both armoured and unarmoured cable

	Outer Circuit					
	Unarmoured			Armoured		
f [Hz]	Z_{ph} [$\Omega\,\mathrm{km}^{-1}$]	R_{ph} [$\Omega\,\mathrm{km}^{-1}$]	L_{ph} [$\mathrm{mH\,km}^{-1}$]	Z_{ph} [$\Omega\,\mathrm{km}^{-1}$]	R_{ph} [$\Omega\,\mathrm{km}^{-1}$]	L_{ph} [$\mathrm{mH\,km}^{-1}$]
20	0.193	0.178	0.594	0.197	0.178	0.670
40	0.239	0.178	0.635	0.252	0.178	0.709
50				0.287	0.179	0.713
60	0.300	0.177	0.644	0.324	0.179	0.715
70	0.335	0.176	0.646	0.363	0.180	0.717
80	0.370	0.176	0.649	0.404	0.181	0.719
100	0.445	0.174	0.652	0.489	0.182	0.722
120	0.523	0.172	0.655	0.577	0.184	0.726

Table 7: Calculated parameters for outer circuit for both armoured and unarmoured cable

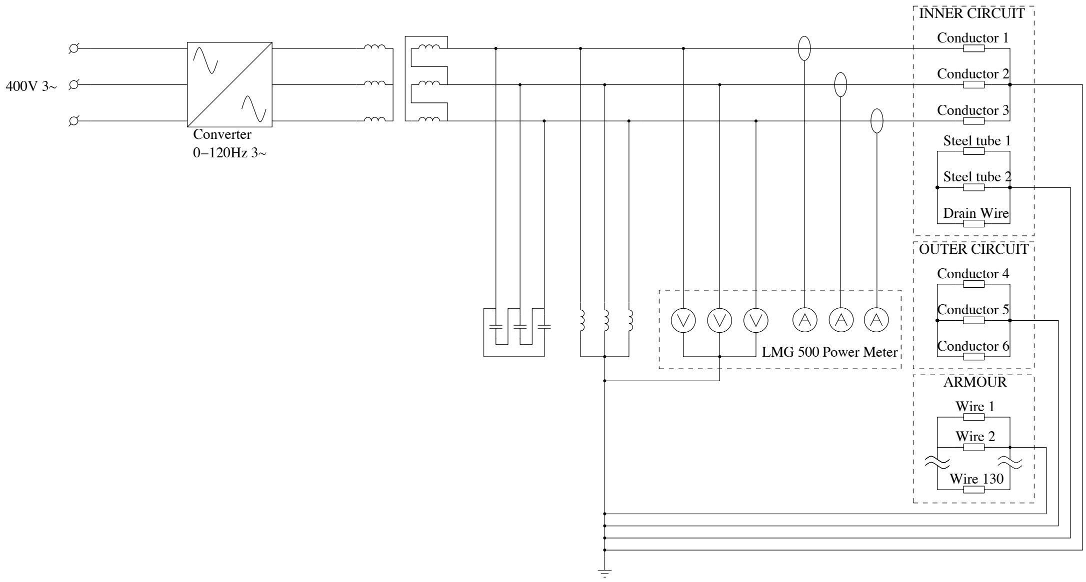

Figure 36: Circuit diagram for test of TXVE 36 kV $6 \times 1 \times 95\,\mathrm{mm}^2$

4 ANALYSIS AND CALCULATIONS

4.1 Induced Loss in Cable Armour

Finite element models are made in order to calculate the loss in the pipes of section 3.3. The only possible method of analysing the effects of circulating currents in a split pipe is with a 3D model. This proved difficult to accomplish due to the enormous amount of memory required for solving the model with a reasonable mesh size.

4.1.1 2D finite element analysis

Models of the intact pipes of section 3.3 are analysed at 50, 120 and 8333 Hz. figure 37 shows the model geometry and plot for intact steel pipe at 8333 Hz. The current is 84 A for all frequencies. The relative permeability for the steel pipes is to be 300. Copper- and carbon steel resistivity is according IEC 60287-1-1; $1.7241 \cdot 10^{-8}\,\Omega\,\mathrm{m}$ and $1.38 \cdot 10^{-7}\,\Omega\,\mathrm{m}$ respectively. The results from the analysis are listed in table 8.

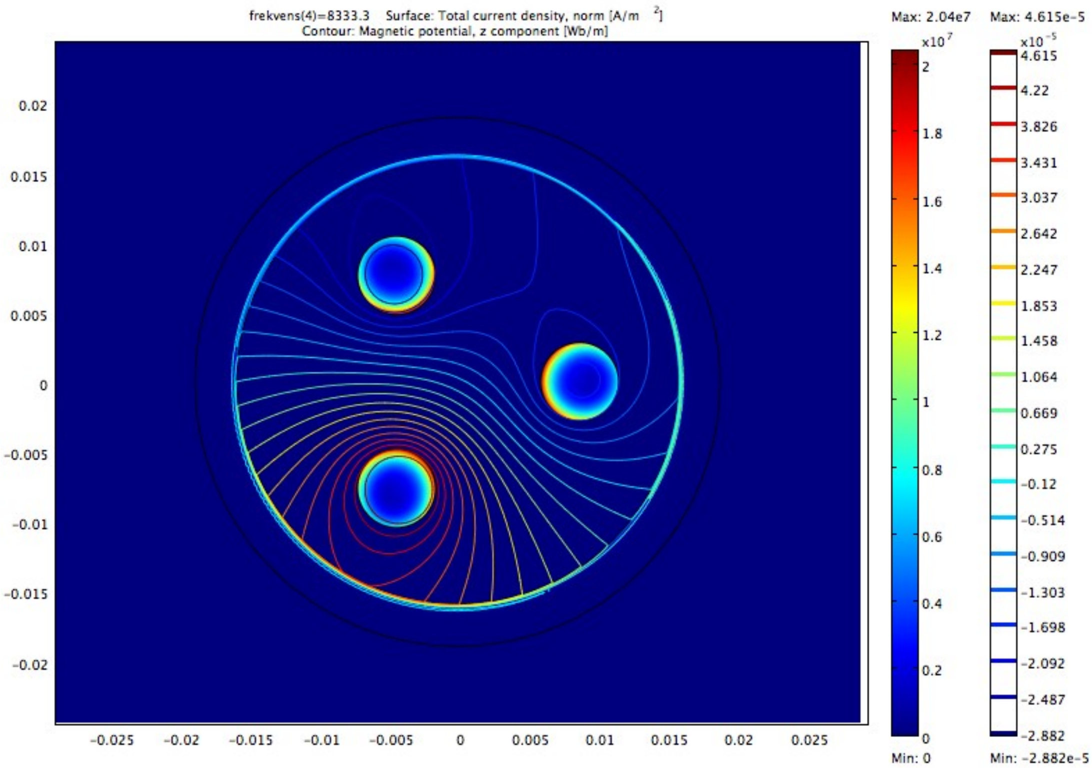

Figure 37: FEA plot for intact steel pipe at 8333 Hz

f [Hz]	Cu Resistive Loss [W]	Fe Resistive Loss [W]
50	0.24	0.03
120	0.69	0.13
8333	5.66	35.44

Table 8: Results of 2D FEA of induced loss in intact pipes

4.1.2 3D finite element analysis

Initial 3D models with physical correct conductors and pipe dimensions proved to memory intensive for the computation server. The maximum amount of physical RAM available is 27 GB. When the models consume all available RAM, the program uses swap disk, resulting in solution times of several days before the simulation tends to fail. In order to reduce the amount of memory required, the conductors are taken out of the equation by using concentrated line-currents on helix shaped lines. The pipe thickness is reduced to two times the skin depth. The depth of the model could not be further reduced, as it already had a minimum depth corresponding to one helix length. figure 38 shows subdomain plots of total current density for both intact and split steel pipes.

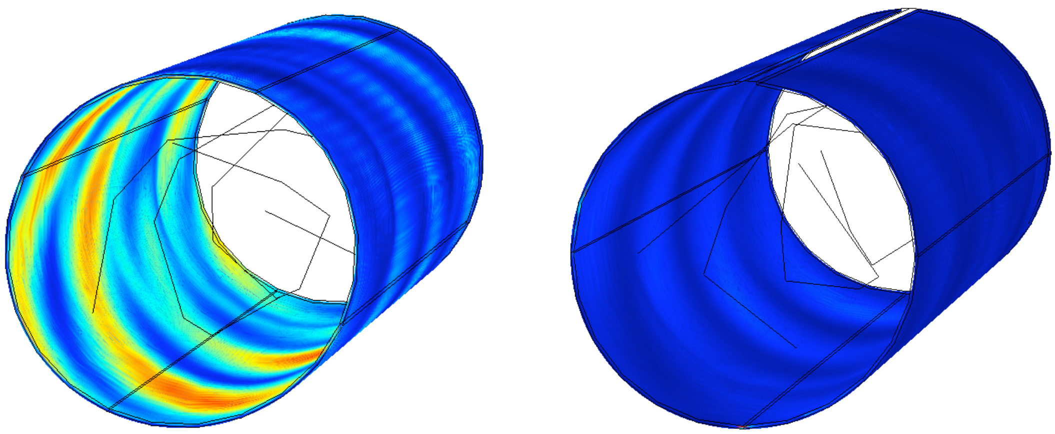

(a) Intact steel pipe (b) Split steel pipe

Figure 38: Subdomain plot av total current density

Only the steel pipes are analysed. The frequency is equal to 8333 Hz. The relative permeability remains unchanged from section 4.1.1. The applied current is still 84 A. The results calculated for 2 meters of pipe are listed below:

- Resistive heating for intact pipe: 15.50 W
- Resistive heating for intact pipe: 14.17 W

4.2 Induced Voltage in Parallel Conductors

4.2.1 2D finite element analysis

To verify the test conducted in section 3.4, a 2D finite element model is analysed. Figure 39 shows the geometry and plot of the model. The depth of the model is, as for the measurements, set to 2 meters. The total induced voltage of the measuring loop is equal to two times the voltage of one conductor of the loop in the model, since the model sees the two small conductors as individual, and not connected at one end. The voltages of the two conductors of the loop are given names (vr and vl) based on equations that describes their currents equal to zero. The three phase circuit in the centre carry a sinusoidal current of $84\,\mathrm{A}_{RMS}$ at a frequency of 8.333 kHz. Equation (9) shows the expression used in- and value obtained from Comsol when calculating the total induced voltage.

$$2\,|vr| = 1.83\,\mathrm{V} \tag{9}$$

Assuming only that one conductor of the measuring loop is used, the geometry of figure 39 will now be equivalent with a single conductor that is twisted around the three-phase circuit at positions 0° and 180° into the plane. For each position the conductor has, there will always be a position 180° opposite to it, that the conductor will be in after 1/2 of a full twist. Using this, the voltage for the entire loop when the three phase circuit is twisted, can now be calculated with equation (10).

$$|vr| - |vl| = 0.010\,\mathrm{V} \tag{10}$$

4.2.2 Analytical calculations

Using the equations described in [4]. The induced voltage for the measuring loop can be expressed as:

$$\Delta U = j\, s\, \mu_0\, f\Big(I_1 \ln\frac{D_1}{0.39\ d} + I_2 \ln\frac{D_2}{0.39\ d} + I_3 \ln\frac{D_3}{0.39\ d}\Big) \tag{11}$$

where s is the length of the conductors, μ_0 is the permeability of vacuum and f is the frequency. $0.39\,d$ is the geometric mean distance of a circular conductor with respect to itself. D_1, D_2 and D_3 are the geometric mean distances between the measuring conductor and the conductors of the three-phase circuit. Inserting values, the induced voltage is calculated:

$$\Delta U = j\,4\cdot 4\pi\,10^{-7}\,8333\Big(-42\ln\frac{26.74}{0.31} + 84\ln\frac{33.57}{0.31} - 42\ln\frac{17.43}{0.31}\Big) = 1.56\,\mathrm{V} \tag{12}$$

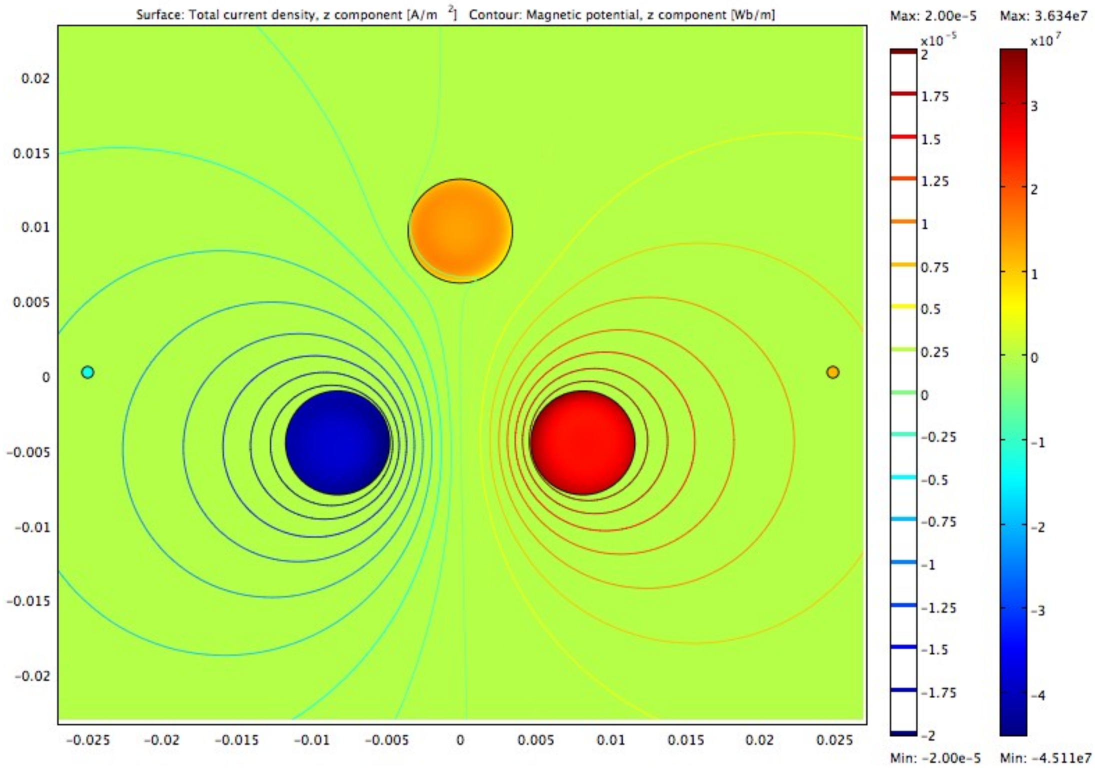

Figure 39: Surface- and contour plot of model

4.3 IEC Calculations of Power Cable

IEC standard 60287-1-1 provides formulas for calculation of current rating and losses in cables. Values calculated by [5], using a computer program based on this standard, are presented for comparison with measured- and computed values for the power cable.

4.3.1 Results

The output file from the program is found in appendix D.1. Based on the computed values, the lead sheet current and armour current is calculated using equations (13) and 14.

$$I_{Lead\,sheet} = \sqrt{\frac{P_{Ph,lead\,sheet}}{R_{DC,lead}} 1000} = \sqrt{\frac{0,0319}{0,276345} 1000} = 10.74409\,[\mathrm{A}] \tag{13}$$

$$I_{Armour} = \sqrt{\frac{P_{Ph,armour}}{R_{AC,armour}} 1000} = \sqrt{\frac{0,0378}{0,064737} 1000} = 24.16404\,[\mathrm{A}] \tag{14}$$

The computed cable parameters from the output file are listed below:

- $R = 0.0672\,[\Omega\,\mathrm{km}^{-1}]$
- $L = 0.4489\,[\mathrm{mH}\,\mathrm{km}^{-1}]$

Dividing the computed armour loss for all three phases by the total loss, the armour loss is found to be 22% of the total loss.

4.4 Finite Element Analysis of Power Cable

4.4.1 Model design

The model is constructed based on the design data listed in table 3 on page 36. The materials electric and magnetic properties are calculated according to [6] at 20°C. Armour wires relative permeability is initially set to be 300.

4.4.2 Physics

Using the results from sections 3.4.4, 3.5.4 and 4.2.1, each armour wire is described with its voltage derived from the current in the wire being equal to zero. This procedure results in a net induced voltage over the wire, but since the current in each wire is set equal to zero, the only contribution to loss in the armour are eddy-currents and hysteresis loss.

4.4.3 Results

Figure 40 shows a surface- and contour plot of magnetic flux density and magnetic potential for the cable. The results are listed in table 9. The cable is analysed with perfect symmetrical currents, and as a consequence the per-phase loss are also symmetrical. The resistance and inductance are calculated in equations (15) and (16). The screen currents equal 10.03 A. The total loss in the armour wires with a relative permeability of 300, is 19.69 W. The influence of armour permeability on the loss and inductance are determined by solving the model for several values of μ_r. The results are listed in table 10.

$$R_{ph} = \frac{|V_1|}{|I_1|} \cos \angle v_1 \, 1000 = 0.05355 \, [\Omega \, \mathrm{km}^{-1}] \tag{15}$$

$$L_{ph} = \frac{|V_1|}{|I_1| \, 2\pi \, f} \sin \angle v_1 \, 1000 = 0.464928 \, [\mathrm{mH} \, \mathrm{km}^{-1}] \tag{16}$$

	Conductor 1		Conductor 2		Conductor 3	
	Magnitude	Angle [°]	Magnitude	Angle [°]	Magnitude	Angle [°]
Voltage [V_{RMS}]	66.65	69.865	66.65	-50.135	66.65	-170.135
Current [A_{RMS}]	51	0	51	-120	51	120
Active Power [W]	1170		1170		1170	
Reactive Power [VAr]	-3191		-3191		-3191	

Table 9: Measured currents, voltages, active- and reactive power

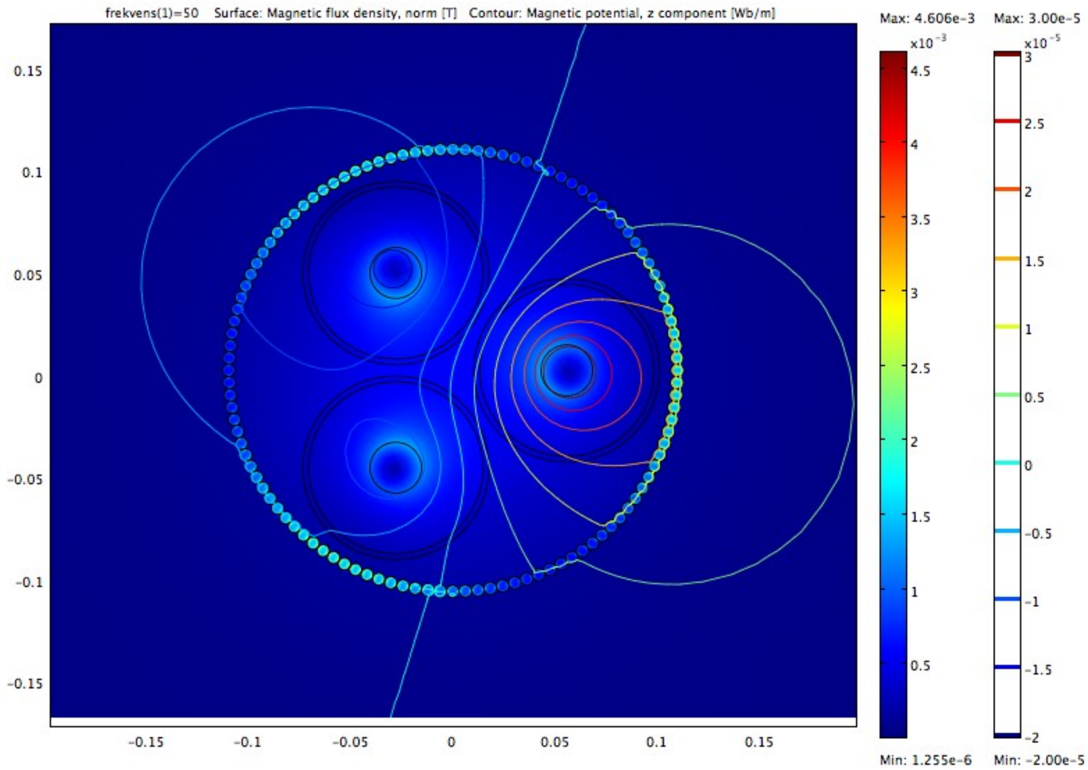

Figure 40: Magnetic flux density and magnetic potential

$\mu_{r,Armour}$	P_{Armour}[W]	L_{Phase} [mH km^{-1}]
50	15.00	0.462106
150	19.30	0.464307
250	19.80	0.464802
300	19.69	0.464928
350	19.44	0.465019
700	16.68	0.465336
1200	13.42	0.465552

Table 10: Resistive loss and inductance for different values of relative armour permeability

4.5 Finite Element Analysis of Power Umbilical

4.5.1 Model design

The model is constructed according to design data listed in appendix C.1. Material properties are based on [6] at 0°C. Conductors are modelled as solid conductors with resistivity according to [6].

4.5.2 Physics

The same physics as described in section 4.4.2, are applied to the armour wires of this model. The model is solved as two individual models. One, where the inner circuit is active, and two, when the outer circuit is active. The physics that apply to these models are not equal in both cases and are therefor listed below:

- Inner Circuit Active

  The conductors of the outer circuit are applied the same physics as the armour wires.

  The steel tubes and drain wire are described with the sum of their currents being equal to zero.

- Outer Circuit Active

  The conductors of the inner circuit together with the steel tubes and drain wire are applied the same physics as the armour wires.

4.5.3 Solving procedure

As for the previous cable, the potential difference applied to the active conductors are functions of perfect symmetrical three phase currents. The current magnitude for a given frequency is set equal to the average current measured at that frequency in section 3.6.4.

4.5.4 Results

Figure 41 shows plots of magnetic flux density and magnetic potential for active inner- and outer circuits at 70Hz. The calculated parameters for armoured cable based on the FEA using Comsol Multiphysics are listed in table 11. Tables 12 and 13 lists the calculated parameters for both armoured and unarmoured cable using Flux 2.5D.

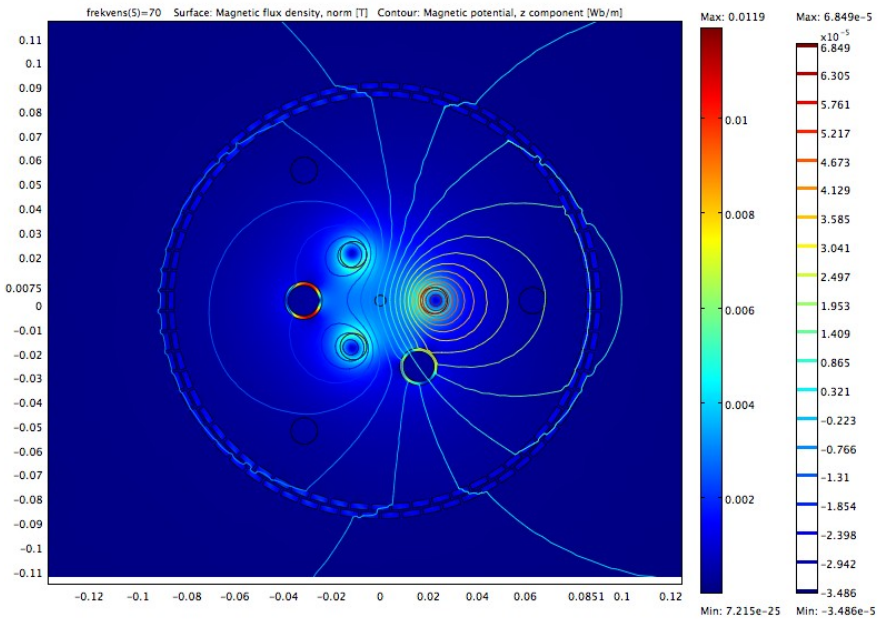

(a) Inner circuit active

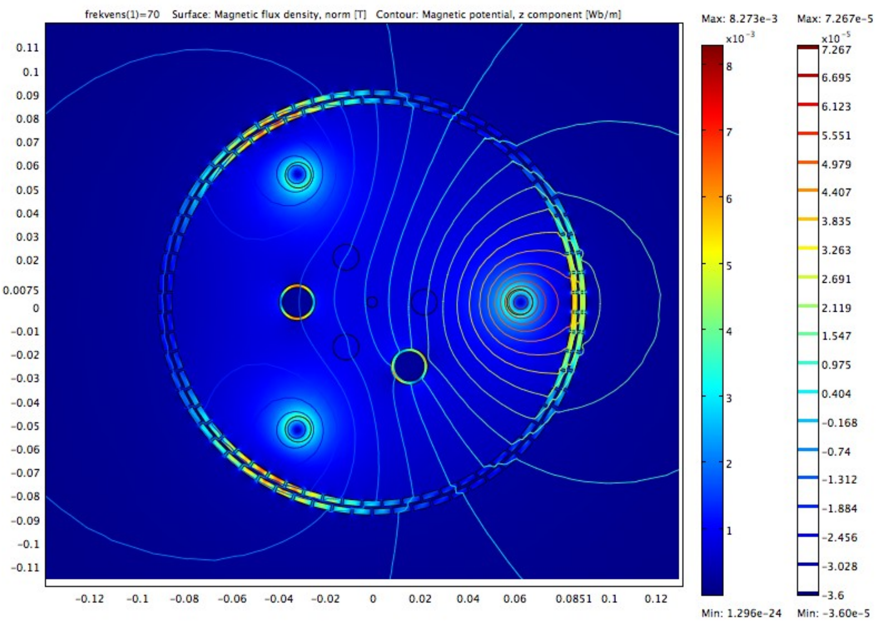

(b) Outer circuit active

Figure 41: Surface- and contour plot of magnetic flux density and magnetic potential

	Armoured Cable					
	Inner Circuit			Outer Circuit		
f [Hz]	Z_{ph} [$\Omega\,\mathrm{km}^{-1}$]	R_{ph} [$\Omega\,\mathrm{km}^{-1}$]	L_{ph} [$\mathrm{mH\,km}^{-1}$]	Z_{ph} [$\Omega\,\mathrm{km}^{-1}$]	R_{ph} [$\Omega\,\mathrm{km}^{-1}$]	L_{ph} [$\mathrm{mH\,km}^{-1}$]
20	0.186	0.177	0.453	0.200	0.178	0.714
40	0.211	0.177	0.453	0.254	0.179	0.714
50	0.227	0.177	0.453	0.288	0.180	0.714
60	0.246	0.178	0.453	0.324	0.181	0.714
70	0.267	0.178	0.453	0.363	0.181	0.714
80	0.289	0.178	0.453	0.402	0.182	0.714
100	0.336	0.179	0.452	0.485	0.184	0.713
120	0.385	0.180	0.452	0.569	0.186	0.713

Table 11: Computed average parameters for armoured cable based on FEA in Comsol Multiphysics

	Inner Circuit					
	Unarmoured			Armoured		
f [Hz]	Z_{ph} [$\Omega\,\mathrm{km}^{-1}$]	R_{ph} [$\Omega\,\mathrm{km}^{-1}$]	L_{ph} [$\mathrm{mH\,km}^{-1}$]	Z_{ph} [$\Omega\,\mathrm{km}^{-1}$]	R_{ph} [$\Omega\,\mathrm{km}^{-1}$]	L_{ph} [$\mathrm{mH\,km}^{-1}$]
20	0,191	0,182	0,452	0,187	0,178	0,459
40	0,215	0,182	0,452	0,212	0,179	0,459
50				0,230	0,179	0,458
60	0,250	0,182	0,451	0,249	0,179	0,458
70	0,270	0,183	0,452	0,270	0,180	0,458
80	0,292	0,184	0,452	0,292	0,180	0,458
100	0,338	0,185	0,451	0,340	0,181	0,458
120 0,388	0,186	0,451	0,390	0,183	0,458	

Table 12: Computed average parameters for inner circuit based on FEA in Flux 2.5D

	Outer Circuit					
	Unarmoured			Armoured		
f [Hz]	Z_{ph} [$\Omega\,\mathrm{km}^{-1}$]	R_{ph} [$\Omega\,\mathrm{km}^{-1}$]	L_{ph} [$\mathrm{mH\,km}^{-1}$]	Z_{ph} [$\Omega\,\mathrm{km}^{-1}$]	R_{ph} [$\Omega\,\mathrm{km}^{-1}$]	L_{ph} [$\mathrm{mH\,km}^{-1}$]
20	0,200	0,182	0,654	0,200	0,178	0,729
40	0,245	0,182	0,654	0,256	0,179	0,729
50				0,291	0,179	0,728
60	0,307	0,183	0,654	0,328	0,180	0,728
70	0,341	0,183	0,654	0,367	0,180	0,728
80	0,376	0,184	0,654	0,408	0,181	0,728
100	0,450	0,185	0,654	0,492	0,182	0,728
120	0,527	0,186	0,653	0,578	0,184	0,727

Table 13: Computed average parameters for outer circuit based on FEA in Flux 2.5D

5 DISCUSSION

5.1 Magnetic Permeability of Armour Wires

5.1.1 Comparison of samples

Samples 2 and 4 experienced a higher magnetization at the same magnetic field before starting to saturate. A chemical analysis of the four samples are displayed in table 14. The two samples are of a lower grade and thereby have less carbon added. Since the permeability is not a dimensioning parameter used during fabrication of the wires, there can be a number of reasons for the difference, ranging from fabrication processes such as heating and cooling, to the chemical compounds of the alloys.

Sample no.	C [%]	Mn [%]	P [%]	S [%]	Si [%]	Cr [%]	Ni [%]	Cu [%]
1	0.310	0.630	0.009	0.018	0.210			0.008
2	0.06	0.42	0.1	0.18	0.15			
3	0.30	0.56	0.008	0.017	0.18			
4	0.047	0.308	0.007	0.014	0.034	0.046	0.082	0.150

Table 14: Chemical analysis of the steel armour wires. Carbon, Manganese, Phosphorus, Sulphur, Silicon, Chromium, Nickel and Copper.

5.1.2 Effects on cable loss and inductance

Table 10 on page 51 lists the resistive loss and average conductor inductance as a function of the permeability. The variation in armour loss is insignificant for a cable with a length of 8.4km. The average conductor inductance increases slightly within the flux density range of the analysed cables.

5.2 Induced Loss in Cable Armour

5.2.1 Measured values and accuracy

Both Computed- and measured values at power frequencies up to 120Hz, prove insignificant amount of loss in armour even though the geometry is optimized for induction.

At a frequency of nearly 10 kHz, the induced loss is considerable both for intact and split pipe. The path of the circulating current is divided by the number of times the conductors are twisted through the pipe when it is split. A slightly reduced loss for split pipes is observed in table 2. This is due to a 2.4% decrease in mass for the steel pipe, and 2.5% decrease for the copper pipe when they are split.

5.2.2 Computed values and accuracy

Computed values of loss deviate from 2D to 3D analysis. This is due to the simplifications of the 3D model, described in section 4.1.2. Although the simplifications made to the 3D model renders the results, at best, questionable – a comparison between the split and intact pipe, yields results, similar to the measurements.

5.2.3 Comparison of Measured and Computed Values

The deviation between the 2D model and the measured values are most likely due to the non-sinusoidal currents produced by the converter. Other possibilities may be the pipes actual resistivity and permeability, compared to that used in the model.

5.3 Induced voltage in parallel conductors

5.3.1 Comparison and accuracy of measured, computed and calculated values

Table 15 lists the resulting induced voltages. The maximum deviation with the measured value as reference is approximately 25%. Most likely reasons for the deviation are asymmetry of conductor geometry and accuracy of oscilloscope at high frequencies and non-sinusoidal voltages. Inter-conductor proximity effect due to high frequencies cause the geometric mean distances to change and are considered to be a plausible reason for the calculated value's deviation.

$\Delta U_{Measured}$ [V]	$\Delta U_{Computed}$ [V]	$\Delta U_{Calculated}$ [V]
2.09	1.83	1.56

Table 15: Comparison of induced voltage

5.4 Power Cable

5.4.1 Comparison and accuracy of measured and computed values

Table 16 shows the measured and computed values. The most likely reason for the deviation of the resistance is the test set-up's artificial neutral point. Observations of asymmetrical phase voltages on a symmetrical load with symmetrical currents corroborate this. Figure 42 shows the measured phase currents and -voltages. A shifting neutral point due to voltage drop over the earthing wires is a likely reason for the deviation.

	R_{Phase} [$\Omega\,\mathrm{km}^{-1}$]	Percent of measured [%]	L_{Phase} [$\mathrm{mH\,km}^{-1}$]	Percent of measured [%]
Measured	0.0585	100	0.466	100
Computed	0.05355	91.5	0.464628	99.7

Table 16: Measured and computed resistance and inductance

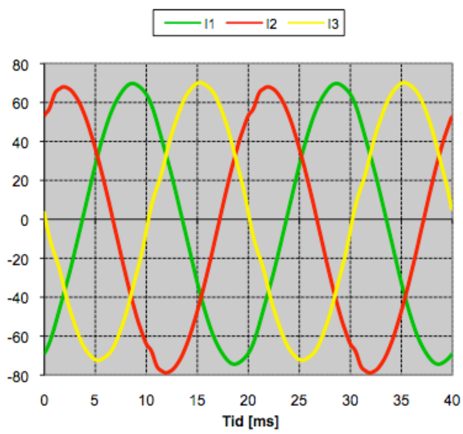

(a) Phase currents

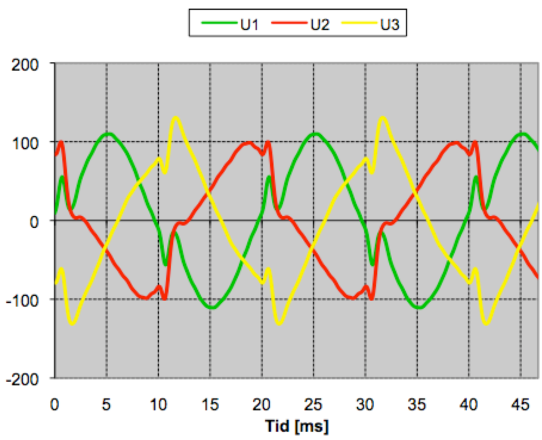

(b) Phase voltages

Figure 42: measured phase currents and -voltages

5.4.2 Comparison with IEC computed values

IEC claims that a current, resulting in a loss of 22% of total loss, floats in the armour. The measurements, analysis and laboratory tests presented in this thesis proves this wrong. The IEC computed conductor resistance deviates with nearly 15% with 114.9% of the measured resistance. The inductance is 96.3% of the measured value.

5.5 Power Umbilical

5.5.1 Comparison and accuracy of measured and computed values

The measured resistance as function of the frequency show the wrong trend. The resistance of the conductors should increase with frequency due to skin effect, but decrease in all cases except for the armoured cables outer circuit. Wrong trend is also observed for the inductance for both inner and outer circuit on armoured and unarmoured cable. The inductance should decrease.

Tables 17 and 18 lists computed values divided by measured values for inner and outer circuit respectively. Measured values at 20 Hz deviate more then values at other frequencies. This has also been the case for measurements on other cables with use of different instruments [5]. Values measured at 60 Hz has the least amount of THD and thus assumed to have best accuracy. Rogowski coils accuracy is frequency dependent. Power meter was found to be overly sensitive to temperature and had to be warmed up before being able to boot. According to technical data in appendix A.5, the instrument should be able to operate from temperatures of 0°C. As for the power cable, the artificial neutral point is constructed with the use of voltage transformers primary windings. It is likely to assume that construction of a stable neutral point failed.

	Inner Circuit					
	Unarmoured			Armoured		
f [Hz]	$Z_{ph,calc}/Z_{ph,meas}$	$R_{ph,calc}/R_{ph,meas}$	$L_{ph,calc}/L_{ph,meas}$	$Z_{ph,calc}/Z_{ph,meas}$	$R_{ph,calc}/R_{ph,meas}$	$L_{ph,calc}/L_{ph,meas}$
20	103,3 %	102,4 %	113,1 %	101,6 %	100,2 %	118,0 %
40	103,3 %	103,0 %	103,1 %	102,6 %	100,6 %	107,8 %
50				102,8 %	101,0 %	105,7 %
60	103,1 %	103,6 %	101,0 %	103,1 %	101,3 %	105,1 %
70	102,9 %	104,3 %	100,8 %	103,1 %	101,6 %	104,4 %
80	102,3 %	104,5 %	100,4 %	103,4 %	102,1 %	104,2 %
100	101,9 %	105,8 %	99,9 %	103,3 %	103,1 %	103,3 %
120	101,5 %	107,4 %	99,3 %	103,1 %	104,3 %	102,7 %

Table 17: Computed values divided by measured values for inner circuit

	Outer Circuit					
	Unarmoured			Armoured		
f [Hz]	$Z_{ph,calc}/Z_{ph,meas}$	$R_{ph,calc}/R_{ph,meas}$	$L_{ph,calc}/L_{ph,meas}$	$Z_{ph,calc}/Z_{ph,meas}$	$R_{ph,calc}/R_{ph,meas}$	$L_{ph,calc}/L_{ph,meas}$
20	103,3 %	102,1 %	110,1 %	101,6 %	100,0 %	108,8 %
40	102,8 %	102,6 %	103,0 %	101,5 %	100,1 %	102,8 %
50				101,4 %	100,1 %	102,2 %
60	102,2 %	103,3 %	101,5 %	101,4 %	100,2 %	101,9 %
70	101,9 %	103,8 %	101,2 %	101,2 %	100,1 %	101,6 %
80	101,6 %	104,4 %	100,8 %	101,1 %	100,1 %	101,3 %
100	101,1 %	106,0 %	100,2 %	100,7 %	100,2 %	100,8 %
120	100,7 %	108,0 %	99,8 %	100,2 %	100,1 %	100,2 %

Table 18: Computed values divided by measured values for outer circuit

6 CONCLUSION

Measurements of armour wire permeability has been performed on four different samples of sub sea armour wires. All samples experience hysteresis loss. Two of the samples had higher remanence magnetization and saturated at higher level of the applied magnetic field. The two samples were of a lower grade with less carbon added. No final conclusion is drawn as to the reason of the difference in magnetization since there could be a number of reasons why and no possible way of checking them. Loss in armour is proved to be virtually unchanged with a considerable variation of permeability using finite element analysis. Inductance increase slightly with a huge increasing permeability. Relative permeability values of armour steel for sub sea power cables in the range of 50 to 500 does not affect the calculations significantly. Traditional value of 300 is within the range and is therefor a good estimate for a wide range of applications.

Evidence that induced voltage and circulating currents in two-layer-two-circuit cables are canceled over every helix length is provided through theory, laboratory small scale tests and measurements on two full scale sub sea cables.

Armour loss is found to be insignificant compared with the vast loss IEC claims present in power cables. Absence of armour wire currents during measurements are further confirmed by laboratory tests- and the theory- of magnetic potential cancellation of twisted circuits. With the cancellation of potential voltage difference over the cable length, follows that there are no source to drive any currents even if the armour is bounded to earth in any possible way. The only source of loss in the armour is eddy-current- and hysteresis- losses.

Equations for use with 2D Finite Element Analysis without any circuit coupling capabilities have been developed and proved accurate compared with measured values.

Values obtained by measurements on the sub sea cables experience deviation from what is expected. An unstable artificial neutral point constructed with inductors is assumed to be the most likely reason for any errors.

Suggested topics for further study, are optimization and development of accurate measuring techniques with special concern for ground reference and measuring equipment's accuracy and reliability at different frequencies.

References

[1] J.S. Barrett and G.J. Anders. Circulating current and hysteresis losses in screens, sheaths and armour of electric power cables – mathematical models and comparison with iec standard 287. *Science, Measurement and Technology, IEE Proceedings*, 144(3):101–110, May 1997.

[2] Hugh D. Young, Roger A. Freedman, Francis W. Sears, and Mark W. Zemansky. *Sears and Zemansky's University physics*. Pearson/Addison-Wesley, San Fransisco, Calif., 12th edition, 2008.

[3] Yanus A. Çengel and Robert H. Turner. *Fundamentals of Thermal-Fluide Sciences*. McGraw-Hill, 2nd edition, 2005.

[4] Arne Nysveen. *Maritime and Offshore Power Systems*. Department of Electric Power Engineering, NTNU, 2008.

[5] Jarle J. Bremnes. Supervisor at nexans.

[6] IEC. Conductors of insulated cables. *IEC 60228*, 11 2004.

A TECHNICAL DATA

A.1 List of Instruments Used at NTNU

Item	*Model*	*Technical Data*	*Local Lab. No.*
Converter	Self manufactured	20kW, 3-phase	P08-0099
DC-link	Self manufactured	AC/DC 400V, 63A, 43kW	R04-0135
Oscilloscope	Tektronix TDS 2014 B	100MHz, 1GS/s, 4 Channel	G04-0343
Oscilloscope	Tektronix TDS 3014 B	100MHz, 1.25GS/s, 4 Channel	G04-0261
Data Logger	Agilent 34970A	300V, 100MΩ, 10MHz, 250S/s	G05-0172
Variac	REO DRRTOS	400V, 25A, 3-phase	B01-0601
Voltage Probe Diff.	Tektronix P5200	1kV, 25MHz	I06-0486
Current Probe	Fluke i1000s AC	10/100/1000A	I04-0407
Thermo Camera	NEC TH7102MX/WX	-40°C - 500°C, 7μm – 14μm	P03-0193
Permeability Tester	Brockhaus Messtechnik	110V, 40A, 10kHz	N01-0020

Table 19: List of instruments used during laboratory work

A.2 List of Instruments Used at Nexans

Item	*Model*	*Technical Data*	*Local Lab. No.*
Frequency Converter	Stadt Sinus K		
Variac	Shuntermann	3x0-400V, 50 Hz	
Power Meter	LMG 500	0.03%, 10MHz, 3MS/s	
Coupling Transformer	Elinduktra	$380 : D/Y - N$	

Table 20: List of instruments used Nexans

A.3 Three-phase Variable Toroidal Auto Transformer (DN 9)

Type DRRTO/DRRTOSpW IP 00

Technische Daten:
Eingangsspannung 3 x 400 V
Ausgangsspannung 3 x 0-400 V
oder 3 x 0-450 V
Frequenzbereich 50-400 Hz
Umgebungstemperatur max. 40°C
Schaltgruppe Y0

Type DRRTO/DRRTOSpW IP 00

Technical data:
Input voltage 3 x 400 V
Output voltage 3 x 0-400 V
or 3 x 0-450 V
Frequency range 50-400 c/s
Maximum ambient temperature 40°C
Connection group Y0

Type DRRTO/DRRTOSpW IP 00

Données techniques:
Tension à l'entrée 3 x 400 V
Tension de sortie 3 x 0-400 V
ou 3 x 0-450 V
Fréquence 50-400 Hz
Température ambiante maximale 40°C
Groupe commutateur Y0

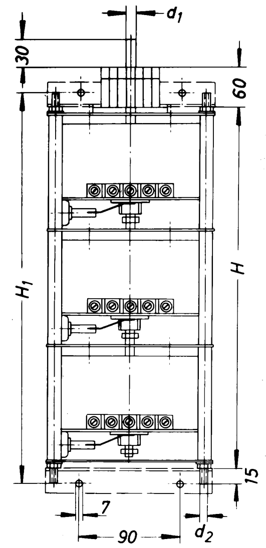

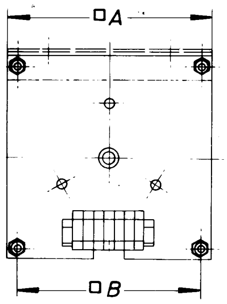

Größe / Type	3 x 0 - 400 V 3 x A	kVA	3 x 0 - 450 V 3 x A	kVA	Abmessungen - Dimensions - Cotes A	B	H	H_1	d_1	d_2	Gewicht Weight Poids kg	Kupfer Copper Cuivre kg
DM 3	0,8	0,55	0,6	0,47							5,5	0,105
DM 4	1,0	0,69	0,9	0,66							7,5	0,195
DM 5	1,6	1,11	1,2	0,93	150	134	330	360	6	M 6	8,5	0,27
DM 6	2,5	1,72	2,0	1,56							10,5	0,42
DM 61	3,2	2,20	2,8	2,19							11,5	0,42
DM 7	4,0	2,76	3,0	2,34			375	405	10	M 6	14,5	0,96
DM 8	6,0	4,14	4,5	3,50			455	485	10	M 10	20,5	1,35
DM 9	8,0	5,52	6,0	4,68	180	160	460	490	10	M 10	26,5	2,1
DM 10	10	6,90	8,0	6,24							32	2,7
DM 11	12	8,28	10	7,80	220	196	485	515	10	M 12	36	3,0
DM 12	15	10,4	12	9,36							40	3,6
DN 7	18	12,4	18	14,0							57	5,7
DN 9	25	17,3	25	19,5	300	249	460	490	10	M 10	72	8,1
DN 10	32	22,1	32	24,9							75	9,9

A.4 Frequency Converter Stadt Sinus

Power Range
• kW connected motor/voltage range
1.3~395kW 200÷240VAC, 3phase
2.2~630kW 380÷415VAC, 3phase
2.5~751kW 440÷460VAC, 3phase
2.7~819kW 480÷500VAC, 3phase
470~981kW 575VAC, 3phase
563~1177kW 660÷690VAC, 3phase
• Degree of protection/size
STAND ALONE: IP20 from Size S05 to Size S40, IP00 Size S50, IP54 from Size S05 to Size S30
BOX: IP54
CABINET: IP24 and IP54.

Motor Specifications
• Motor voltage range/precision
0÷Vmains, +/-2%
• Current/torque to motor/time
105÷200% for 2min. every 20min. up to S30.
105÷200% for 1min. every 10min. from S40.
• Starting torque/max. time
240% for a short time
• Output frequency/resolution
0÷800Hz (120Hz for VTC SW), resolution 0.01Hz
• Braking torque
DC braking 30%*Cn
Braking while decelerating up to 20%*Cn (with no braking resistor)
Braking while decelerating up to 150%*Cn (with braking resistors)
• Adjustable carrier frequency with silent random modulation.
IFD SW:
S05÷S15 = 0.8÷16kHz
S20 = 0.8÷12,8kHz
S30 = 0.8÷10kHz (5kHz for 0150 and 0162)
≥S40 = 0.8÷4kHz

VTC SW:
5kHz

Mains
• VAC supply voltage/tolerance
200÷240VAC, 3phase, -15% +10%
380÷500VAC, 3phase, -15% +5%
500÷575VAC, 3phase, -15% +10%
660÷690VAC, 3phase, -15% +10%
• VDC supply voltage/tolerance
280÷360VDC, -15% +10%
530÷705VDC, -15% +5%
705÷810VDC, -15% +10%
930÷970VDC, -15% +10%
• Supply frequency (Hz)/tolerance
50÷60Hz, +/-10%

Environmental Requirements
• Ambient temperature
0÷40°C no derating
(40°C to 50°C derating 2% of rated current every degree beyond 40°C)
• Storage temperature
-25÷+70°C
• Humidity
5÷95% (non condensing)
• Altitude
Up to 1000m a.s.l.
For higher altitudes, derate the output current of 2% every 100m beyond 1000m (max. 4000m)
• Vibrations
Lower than 5.9m/sec^2 (=0.6G)
• Installation environment
Do not install in direct sunlight and in places exposed to conductive dust, corrosive gases, vibrations, water sprinkling or dripping (if not protected by an adequate degree of protection). Do not install in salty environments.
• Operating atmospheric pressure
86÷106kPa
• Cooling system:
Forced air-cooling

A.5 Precision Power Meter LMG500

Measuring accuracy

Accuracy		± (% of measuring value + % of measuring range)									
		DC	0.05Hz..45Hz	**45Hz..65Hz**	65Hz..3kHz	3kHz..15kHz	15kHz..100kHz	100kHz..500kHz	500kHz..1MHz	1MHz .. 3MHz	3MHz .. 10MHz
Voltage	U*	0.02+0.06	0.02+0.03	**0.01+0.02**	0.02+0.03	0.03+0.06	0.1+0.2	0.5+1.0	0.5+1.0	3+3	f/1MHz*1.2 + f/1MHz*1.2
	Usensor	0.02+0.06	0.015+0.03	**0.01+0.02**	0.015+0.03	0.03+0.06	0.2+0.4	0.4+0.8	0.4+0.8	f/1MHz*0.7 + f/1MHz*1.5	f/1MHz*0.7 + f/1MHz*1.5
Current	I* (20mA .. 5A)	0.02+0.06	0.015+0.03	**0.01+0.02**	0.015+0.03	0.03+0.06	0.2+0.4	0.5+1.0	0.5+1.0	f/1MHz*1 + f/1MHz*2	-
	I* (10A .. 32A)					0.1+0.2	0.3+0.6	f/100kHz*0.8 + f/100kHz*1.2	-	-	-
	I HF					0.03+0.06	0.2+0.4	0.5+1.0	0.5+1.0	f/1MHz*1 + f/1MHz*2	-
	I sensor					0.03+0.06	0.2+0.4	0.4+0.8	0.4+0.8	f/1MHz*0.7 + f/1MHz*1.5	f/1MHz*0.7 + f/1MHz*1.5
Power	U* / I* (20mA .. 5A)	0.032+0.06	0.028+0.03	**0.016+0.02**	0.028+0.03	0.048+0.06	0.24+0.3	0.8+1.0	0.8+1.0	f/1MHz*3.2 + f/1MHz*2.5	-
	U* / I* (10A .. 32A)					0.104+0.13	0.32+0.4	f/100kHz*1 + f/100kHz*1.1	-	-	-
	U* / I HF					0.048+0.06	0.24+0.3	0.8+1.0	0.8+1.0	f/1MHz*3.2 + f/1MHz*2.5	-
	U* / I sensor					0.048+0.06	0.24+0.3	0.72+0.9	0.72+0.9	f/1MHz*3 + f/1MHz*2.3	f/1MHz*1.5 + f/1MHz*1.4
	U sensor / I* (20mA .. 5A)		0.024+0.03		0.024+0.03	0.048+0.06	0.32+0.4	0.72+0.9	0.72+0.9	f/1MHz*1.4 + f/1MHz*1.8	-
	U sensor / I* (10A .. 32A)					0.104+0.13	0.4+0.5	f/100kHz*1 + f/100kHz*1	-	-	-
	U sensor / I HF					0.048+0.06	0.32+0.4	0.72+0.9	0.72+0.9	f/1MHz*1.4 + f/1MHz*2	-
	U sensor / Isensor					0.048+0.06	0.32+0.4	0.64+0.8	0.64+0.8	f/1MHz*1.12 + f/1MHz*1.5	f/1MHz*1.12 + f/1MHz*1.5

additional measurement uncertainty in the ranges 10A to 32A: $\pm I^2_{trms} \cdot 30\mu A/A^2$

Accuracies based on:	1. sinusoidal voltage and current 2. ambient temperature 23 ± 3 °C 3. warm up time 1h 4. definition of power range as the product of current and voltage range, $0 \leq \lvert\lambda\rvert \leq 1$, ($\lambda$=Power factor=P/S) 5. calibration interval 12 month
Other values	All other values are derived from the current, voltage and active power values. Accuracies for derived values depend on the functional relationship (e.g. $S = I * U$, $\Delta S/S = \Delta I/I + \Delta U/U$)
Isolation	All current and voltage inputs isolated against each other, against remaining electronic and against earth max. 1000V/CAT III resp. 600V/CAT IV
Synchronization	The measurement is synchronized on the signals period. There is a choice to determine the period from „line", „extern", u(t), i(t) as well as their envelopes, combined with settable filters. By this very stable readings are achieved, even at signals of pulse width modulated frequency inverters and amplitude modulated electronic ballasts
Harmonic analysis (option CE Harm L50-09)	Measuring of current and voltage with evaluation in full compliance with EN61000-3-2/-12, measurement according to EN61000-4-7
Harmonic analysis (option Harm100 L50-08)	Analysis of current, voltage (incl. phase angle) and power up to 99th harmonics, in total 100 harmonics including DC component. Fundamental in the range from 0.1Hz to 1.2 kHz. Analysis up to 10kHz (50kHz without antialiasing filter). By integer divider (1...128) a new reference fundamental can be created as to detect interharmonics. Externally on PC up to 1MHz with LMG-CONTROL software.
Flicker measuring (option L50-04)	Flicker meter according to EN61000-4-15 with evaluation in full compliance with EN61000-3-3/-11
Transients (option L50-05)	Detecting and recording of transients >330ns
Scope function (standard)	Graphical representation of sampled values versus time
Plot function (standard)	Time (Trend) diagram of max. 4 readings, minimal resolution 50ms, respectively 10ms in 50Hz half-wave (flicker) mode
Star delta conversion (option L50-06)	Sums and differences between channels on sample basis
Computer interfaces	**RS232 (standard)** and **IEEE488.2 (option L50-01)**, additional **USB 2.0 Typ B (L50-O2USB), Ethernet 10/100 Base-T RJ45 (option L50-Z318)** available. Only one interface can be used at the same time
Remote control	All functions can be remote-controlled, keyboard lock for measuring parameters
Output data	Output of all readings, data formats BIN/ASCII, SCPI command set
Transfer rate	RS232: max.115200 Baud, IEEE488.2: max. 1MByte/s
USB-stick connector (option L50-O2USB)	For logging data
Printer interface (standard)	Parallel PC-Printer interface with 25-pin SUB-D socket, printing measuring values, tables and graphics to matrix, inkjet or laser printers
Processing signal interface (option L50-03)	2 x 25 pin SUB-D socket with: • 8 analog inputs for process magnitudes (24Bit, ±10V) • 8 analog outputs (14Bit, ±10V) • 8 digital inputs • 8 digital outputs • 2 input for frequency (0.05Hz...6MHz) and rotation direction • in- and outputs are isolated against other electronics (test voltage 500V)
Other data	
Dimensions/Weight	• Bench case 1 to 4 channels W 433mm x H 148mm x D 506mm / about 12kg • Bench case 1 to 8 channels W 433mm x H 283mm x D 506mm / about 23kg • Accessories: brackets for 19" rack, 84PU, 3HU, D 464mm
Protection class	EN61010 (IEC61010, VDE0411), protection class I
Electromagnetic compatibility	EN61326
Protection system	IP20 in accordance to EN60529
Operating/storage temperature	0...40°C/-20...50°C
Climatic class	Normal environment conditions according to EN61010
Power supply	100...240V, 50...60Hz, max. 150W (4 channel device), max. 300W (8 channel device)
LMG500 application software	(Name of software is equal with order number, please request detailed data sheets)
LMG-CONTROL	Individual configuration of measurement, using all features of the LMG500, spectral analysis, remote of LMG500, storage in MS Excel readable format (e.g. CSV-file)
Waveform analysis module	Logging and analysis of all sampling values
PQA-SOFT	Software especially designed for power quality analysis (acc. EN50160), easy configuring of measurement in a few steps
SYS61K-1/3-SOFT	Control and evaluation software for test systems of harmonics and flicker according to EN61000-3-2/-3/-11/-12

Voltage measuring ranges U*												
Nominal value /V	3	6	12.5	25	60	130	250	400	600	1000		
Maximum trms value /V	3.6	7.2	14.4	30	66	136	270	560	999	1001		
Maximum peak value for full scale /V	6	12	25	50	100	200	400	800	1600	3200		
Input impedance	>4.5MΩ || <3pF											
Current measuring ranges I*												
Nominal value /A	20m	40m	80m	150m	300m	600m	1.2	2.5	5	10	20	32
Maximum trms value /A	37m	75m	150m	300m	600m	1.25	2.5	5	10	20	32	32
Maximum peak value for full scale /A	56m	112m	224m	469m	938m	1.875	3.75	7.5	15	30	60	120
Shunt impedance		560mΩ			68mΩ			7.5mΩ			2mΩ	
Current measuring ranges I_{HF}*												
Nominal value /A	150m	300m	600m	1.2								
Maximum trms value /A	225m	450m	900m	1.8								
Maximum peak value for full scale /A	313m	625m	1.25	2.5								
Shunt impedance	0.1Ω											
Sensor inputs U_{Sensor},I_{Sensor}												
Nominal value /V	30m	60m	120m	250m	500m	1	2	4				
Maximum trms value /V	37m	75m	150m	300m	600m	1.2	2.5	5				
Maximum peak value for full scale /V	62m	125m	250m	500m	1	2	4	8				
Input impedance	100kΩ || 34pF											

A.6 Three-phase Variable Auto Transformer

Schuntermann Transformatoren GmbH			
40721 Hilden			
Nr. 5130117021		**Bv.** 2-301-03-005	
Typ. YR 400 / 50		Nach **VDE**	
Leistung	**VA**	50 **Hz**	**Bau Jahr** 02.2003
Eingang	3x400		**V**
3P/N/PE			**A**
Ausgang	3x0-400		**V**
3P/N/PE	50		**A**
Schutz Art **IP** 21			

A.7 Coupling Transformer

ELINDUKTRA-SUNDBERG AB Fack, 695 01 LAXÅ	Uttagsschema för transformatorer	Order nr. 570656 Kund:
	Typ TLFO 27/3286	Nr. 21779 Dat. 76 04 13

Kopplingsart enl. SEN 270101	yD 1 YyO
Vektordiagram	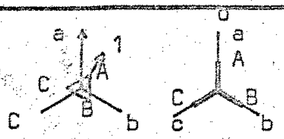

Lindningarna äro sedda från respektive kopplingssidor	Anslut. genomf.	Koppl.	Förbind	Omk. Förb.	Omk. Läge	Volt
	a b c	y				380
	A B C	D	B12-C1 A12-B1 C12-A1	4-5 9-10		2200
				3-5 9-10		2100
				3-6 9-10		2000
				2-6 9-10		1900
				2-6 8-10		1800
	A B C	Y-N	A12-C12 B12-C12	3-6 9-10		3465
				2-6 9-10		3308
				2-6 8-10		3150
				2-6 8-11		2992
				2-6 7-11		2835

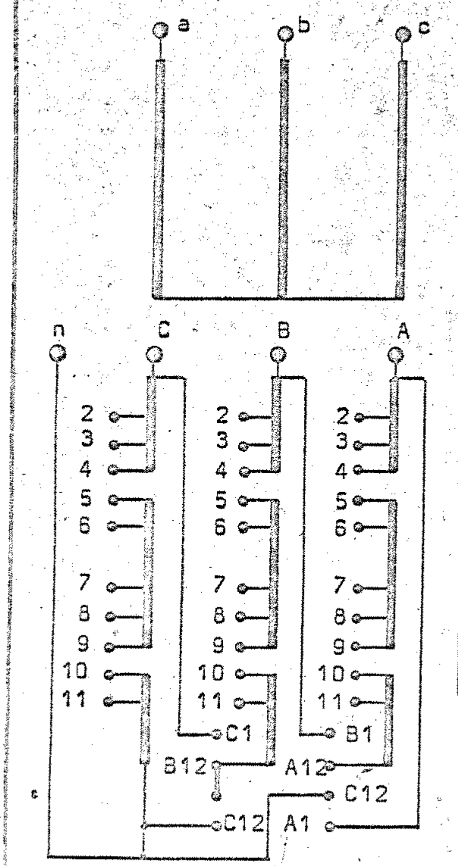

A.8 Three-phase High Voltage Power Capacitors

TECHNICAL DATA

Type:	impregnated all-film dielectric
Rated voltages:	3300 V or 6600 V
Rated frequency:	50 Hz or 60 Hz
Average losses:	0.15 W/kvar
Dielectric liquid:	non-pcb
All-film dielectric:	polypropylene
Temperature category:	-40°C/C (+50°C) IEC 60871-1
Standards to be applied:	IEC, ANSI/IEEE, CSA,
Standard colour:	grey (RAL 7035)

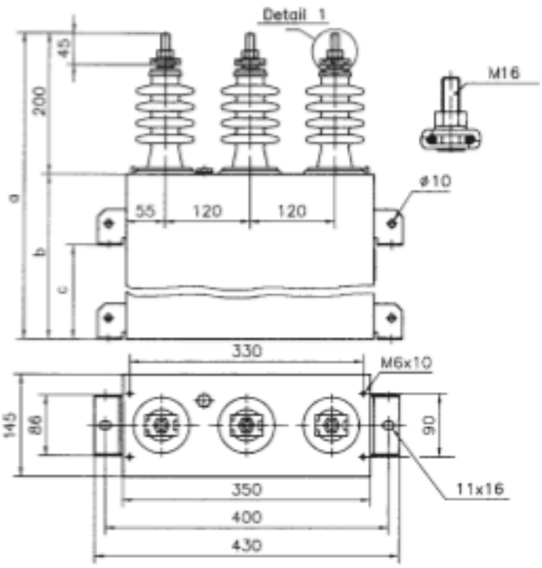

DIELECTRIC LIQUID

The dielectric liquid is specially made for power capacitors and it is chosen by Nokian Capacitors because of its excellent electrical properties and heat stability at both lower and elevated temperatures. It is non-pcb, non-chlorine and biodegradable.

- The capacitor units are equipped with weld type porcelain bushings.
- Capacitor containers are made of stainless steel and painted with suitable primer coat prior to finishing coat to ensure prolonged durability.
- Capacitors for specific purposes can be designed and manufactured to meet customers' requirements.

Standard types

Type	**Power** kvar		**Voltage** V	**Dimensions** mm			**Weight** kg
	50 Hz	60 Hz		a	b	c	
QYLP	50	60	3300/6600	450	260	160	23
QYLP	75	90	3300/6600	490	300	200	26
QYLP	100	120	3300/6600	550	360	260	30
QYLP	150	180	3300/6600	650	460	360	36
QYLP	200	240	3300/6600	770	580	480	44
QYLP	250	300	3300/6600	890	700	600	52
QYLP	300	360	3300/6600	1010	820	720	60
QYLP	350	420	3300/6600	1110	920	820	66

B CIRCUIT DIAGRAMS

B.1 LabVIEW Virtual Instruments Schematics

Block Diagram

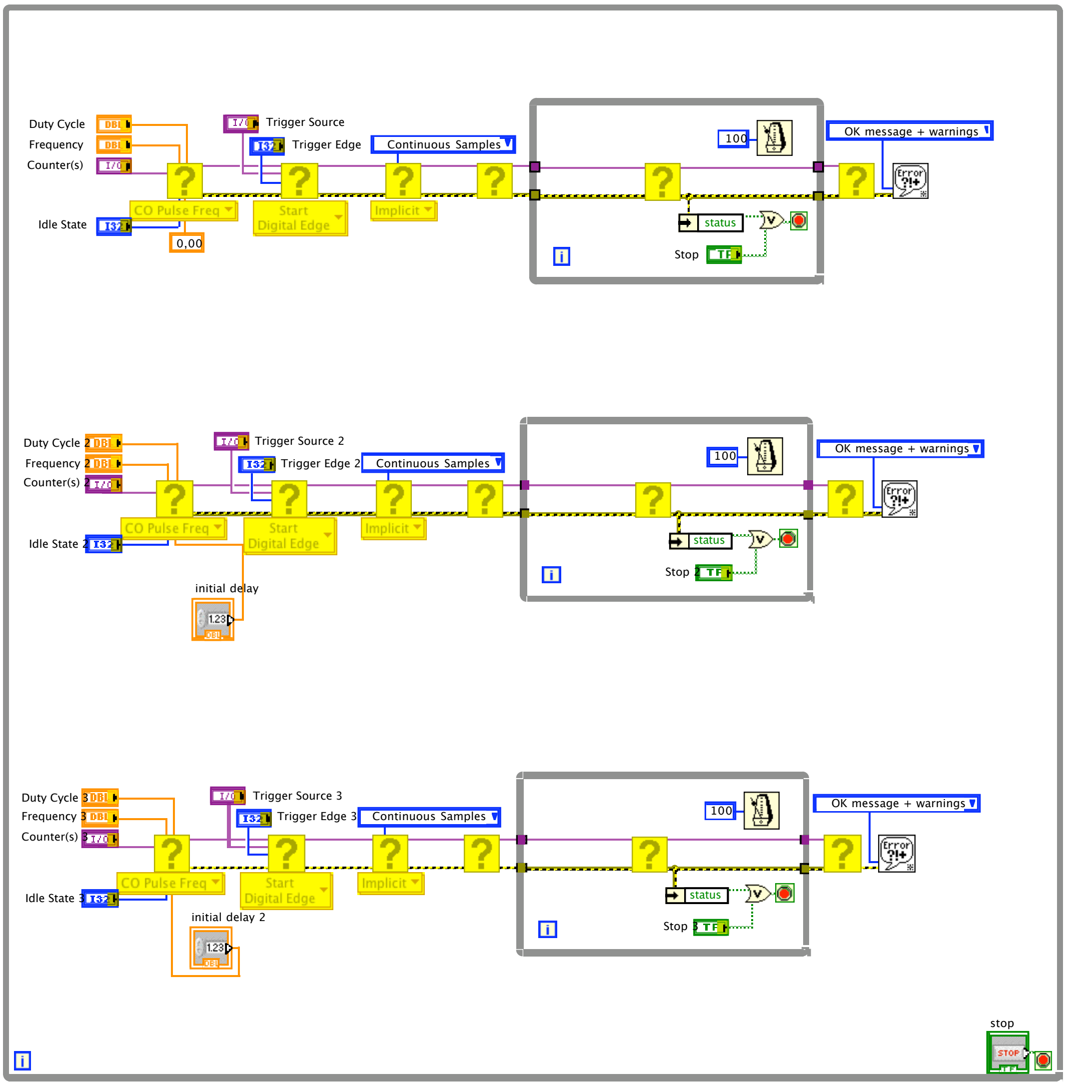

Front Panel

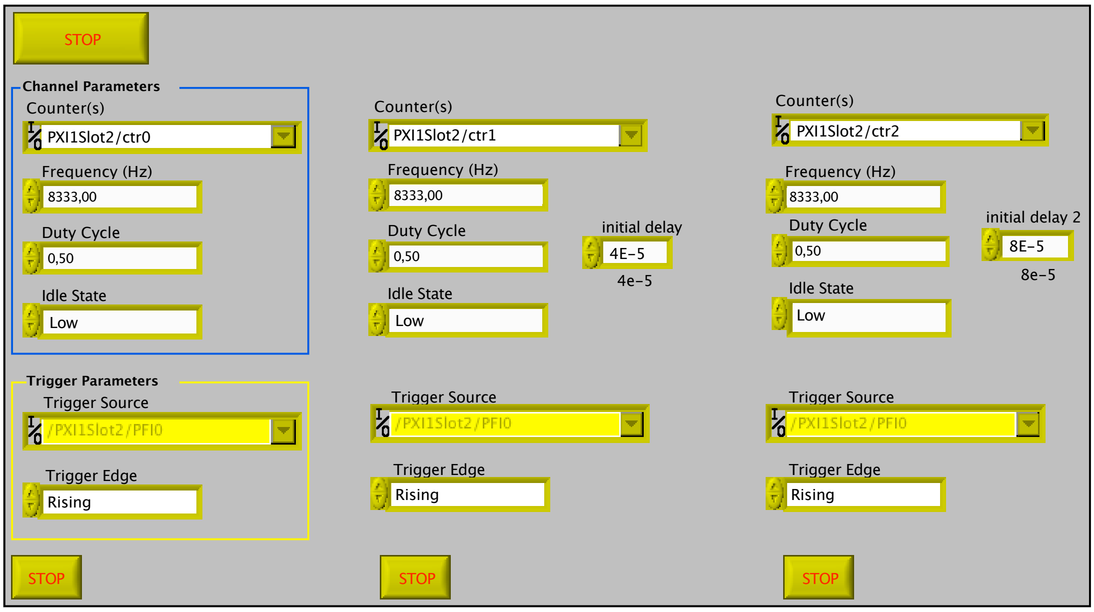
STOP
Channel Parameters
Counter(s)
PXI1Slot2/ctr0
Frequency (Hz)
8333,00
Duty Cycle
0,50
Idle State
Low
Trigger Parameters
Trigger Source
/PXI1Slot2/PFI0
Trigger Edge
Rising
STOP
Counter(s)
PXI1Slot2/ctr1
Frequency (Hz)
8333,00
Duty Cycle
0,50
initial delay
4E-5
4e-5
Idle State
Low
Trigger Source
/PXI1Slot2/PFI0
Trigger Edge
Rising
STOP
Counter(s)
PXI1Slot2/ctr2
Frequency (Hz)
8333,00
Duty Cycle
0,50
initial delay 2
8E-5
8e-5
Idle State
Low
Trigger Source
/PXI1Slot2/PFI0
Trigger Edge
Rising
STOP

C DESIGN DATA

C.1 Cross Section of TXVE $36\,\mathrm{kV}\ 6 \times 1 \times 95\,\mathrm{mm}^2$

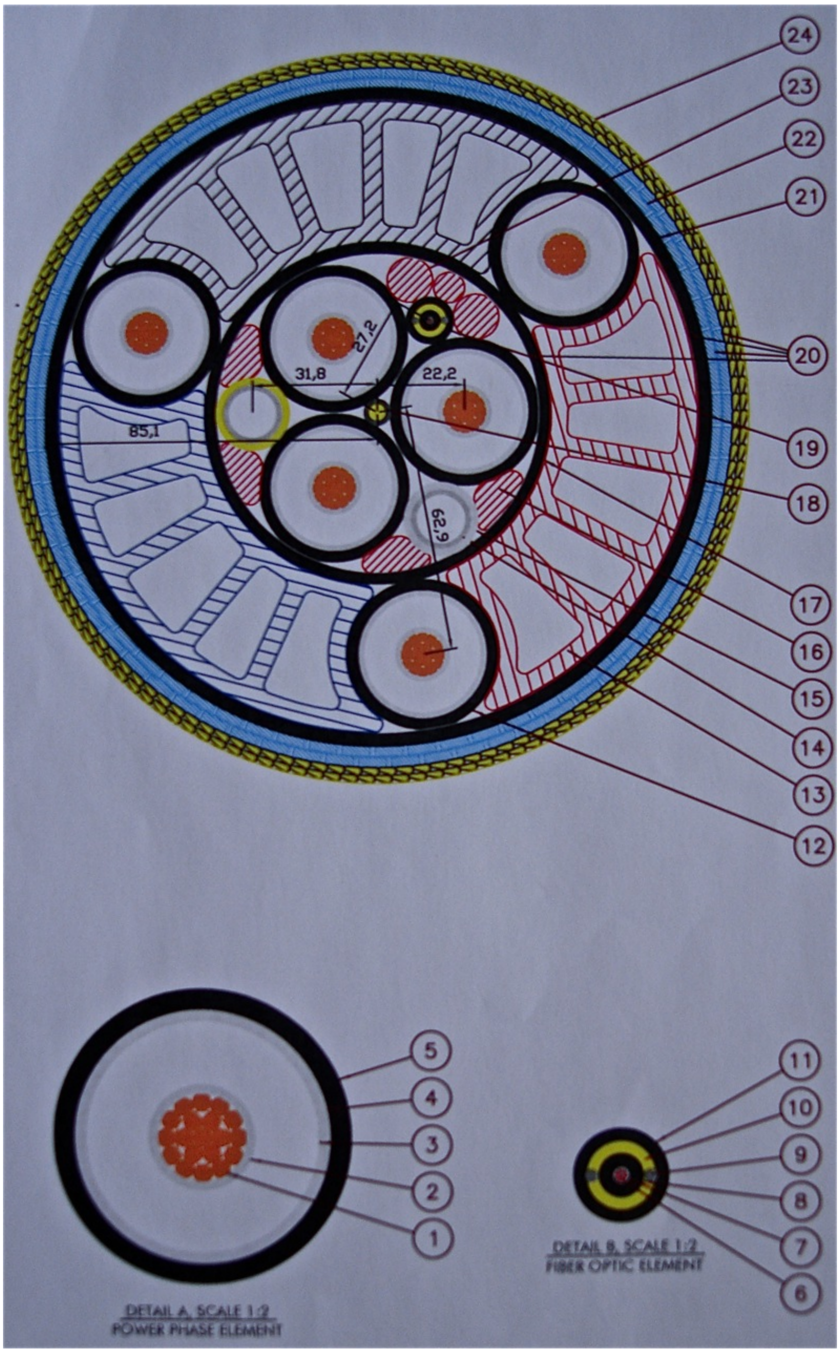

	ITEM	QTY.	DESCRIPTION	NOM. THICKNESS	NOM. DIAMETER
	24		OUTER COVER, PP-YARN (TWO LAYERS)		APP. 189
	23	3	FILLER FILLER, POLYPROPYLENE		
	22		GALVANIZED ARMOUR WIRE, 2 LAYERS (64+66)	2.5 X 7.5	
	21		SEMI-CONDUCTING SHEATH (PE81)	3.0	
	20		WRAPPING		
	19	1	FO CABLE (8 FIBRES), ARAMID ARMOURED (DETAIL B)		12.0
	18		DRAIN WIRE, 16mm² WITH SEMI-CONDUCTING SHEATH		6.6
	17		SEMI-CONDUCTING SHEATH (PE81)	2.5	
	16	2	FILLER ELEMENT, POLYPROPYLENE		
	15		SHEATH, HDPE (PE102)	1.7	
	14	2	SUPER DUPLEX STEEL TUBE 1/2", 345bar	1.46	15.62
	13	3	PROFILED FILLER (HDPE)		
	12	6	HV POWER PHASE 36kV, 95mm² (DETAIL A)		37.9
DETAIL B FIBER OPTIC ELEMENT	11		OUTER SHEATH, SEMI-CONDUCTING PE		12.0
	10		ARMOURING, ARAMIDE		9.0
	9	2	SEMICONDUCTING FILLERS		
	8		INNER SHEATH, SEMI-CONDUCTING PE		6.0
	7		STEEL TUBE, AISI 316L	0.2	2.3
	6	8	OPTICAL FIBRES		0.25
DETAIL A POWER PHASE ELEMENT	5		SEMI-CONDUCTING POLYETHYLENE (PE81)	2.5	37.9
	4		SEMI-CONDUCTING, CROSS-LINKED COPOLYMER	1.5	32.9
	3		CROSS-LINKED POLYETHYLENE (XLPE)	8.0	
	2		SEMI-CONDUCTING, CROSS-LINKED COPOLYMER	1.0	
	1	1	95 mm², STRANDED AND COMPaCTED ANNEALED COPPER		11.5

D COMPUTED VALUES

D.1 Current Rating Output File

```
OUTPUT FROM PROGRAM CURRENT RATING


Cable:
Project:

DESIGN DATA
-----------

LNR       MATERIAL                    N   W/OD    T      GAP/OVL DIA     MASS

       CONDUCTOR 500 mm2 CU              26,5                  26,5    4350
30012588  TETNINGSMASSE                                      26,5    71,85
20016004  PEX 75 SUPERSMOOTH HALVLEDER       29,5    1,5             29,5    163,59
20015991  PEX 24                         79,5    25            79,5    3937,99
20016004  PEX 75 SUPERSMOOTH HALVLEDER       82,5    1,5             82,5    438,96
30013412  SVELLEBÅND HALVLEDENDE        2    70      0,5     -50     85,3    105,43
30014896  BLY 1/2C                        90,9    2,8            90,9    8811,39
20016007  PE 81 SORT TERMOPLASTISK HALV              2,8             96,5    815,99
30012626  NYLONBÅND CT 59/113           2    70      0,17            208,61  170,12
30012781  POLYPROPYLENGARN 5500 TEX SOR 96   4,35    2               212,61  726,54
30014778  STÅLTRÅD GALVANISERT GRADE 34 112          6               224,61  25003,3
30012781  POLYPROPYLENGARN 5500 TEX SOR 105  4,35    2,5             229,61  753,98
30012781  POLYPROPYLENGARN 5500 TEX SOR 128  4,35    2,5             234,61  918,58


INPUT DATA
----------

Cable Type                        :TKRA 245kV 3x1x500mm2 KQ
Number of cables                  :1
Maximum conductor temperature (C)   :90
Voltage max phase - phase (kV)      :245
Voltage operating phase - phase (kV):12
Voltage operating phase - gnd (kV)  :6,9
Frequency (Hz)                    :50
Ambient temperature (C)           :20
Sp. thermal res. outer media(K.m/W) :0,001
Convergence criteria Current (A)    :0,05
Convergence criteria Temp. (C)      :0,01
Coupling of sheats                :Both ends


LAYING
------

Outer media                       :Soil

Laying                            :Direct

CABLE COORDINATES
-----------------

GROUP          XSP    YSP    XSP    YSP    XSP    YSP(m)
Group 1          0      0,01


RESULTS: CURRENT RATING CALCULATIONS
------------------------------------

Rated Current (A)                 :50,03

R DC Conductor 20oC (ohm/km)        :0,0366
R DC Conductor op. temp. (ohm/km)   :0,0366179
R AC Conductor op. temp. (ohm/km)   :0,0393427
Skin effect factor                :0,0584693
```

Proximity effect factor :0,0159436

Capacitance insulation (uF) :0,1401
Charging current (A/km) :0,30493
R DC 20 oC BLY 1/2C :0,27628
R AC 20 oC STÅLTRÅD GALVANISERT GRA :0,064731

R DC Op. Temp BLY 1/2C :0,276345
R AC Op. Temp STÅLTRÅD GALVANISERT :0,064737

Thr. res. insulation T1 (m K/W) :0,6645
Thr. res. bedding T2 (m K/W) :0,0965
Thr. res. outer covering T3 (m K/W) :0,0416
Thr. res. outer media T4 (m K/W) :0,0003

Conductor temperature (oC) :20,12
Temperature (oC) BLY 1/2C :20,06
Temperature (oC) STÅLTRÅD GALVANISE :20,02
Cable surface temperature (oC) :20

Resulting lossfactor (Lambda1) :0,3246
Resulting lossfactor (Lambda2) :0,3844
Loss in conductor pr. phase (W/m) :0,0984
Loss pr. phase (W/m) BLY 1/2C :0,0319
Loss pr. phase (W/m) STÅLTRÅD GALVA :0,0378
Sum losses per cable (W/m) :0,5043

Conductor Inductance (mH/km) :0,4489
Cable impedance (Ohm/km) :0,0672+0,141j
Cable impedance average(Ohm/km) :0,0672+0,141j

RESULTS: VOLTAGE GRADIENT CALCULATIONS

	U	Us	U0	Um
Voltage (kV)	220	1050	0	245
Inner Gradient (kV/mm)	8,69	71,81	0	9,67
Outer Gradient (kV/mm)	3,22	26,65	0	3,59

D.2 Mu Curve and Hysteresis Curve for Sample 1

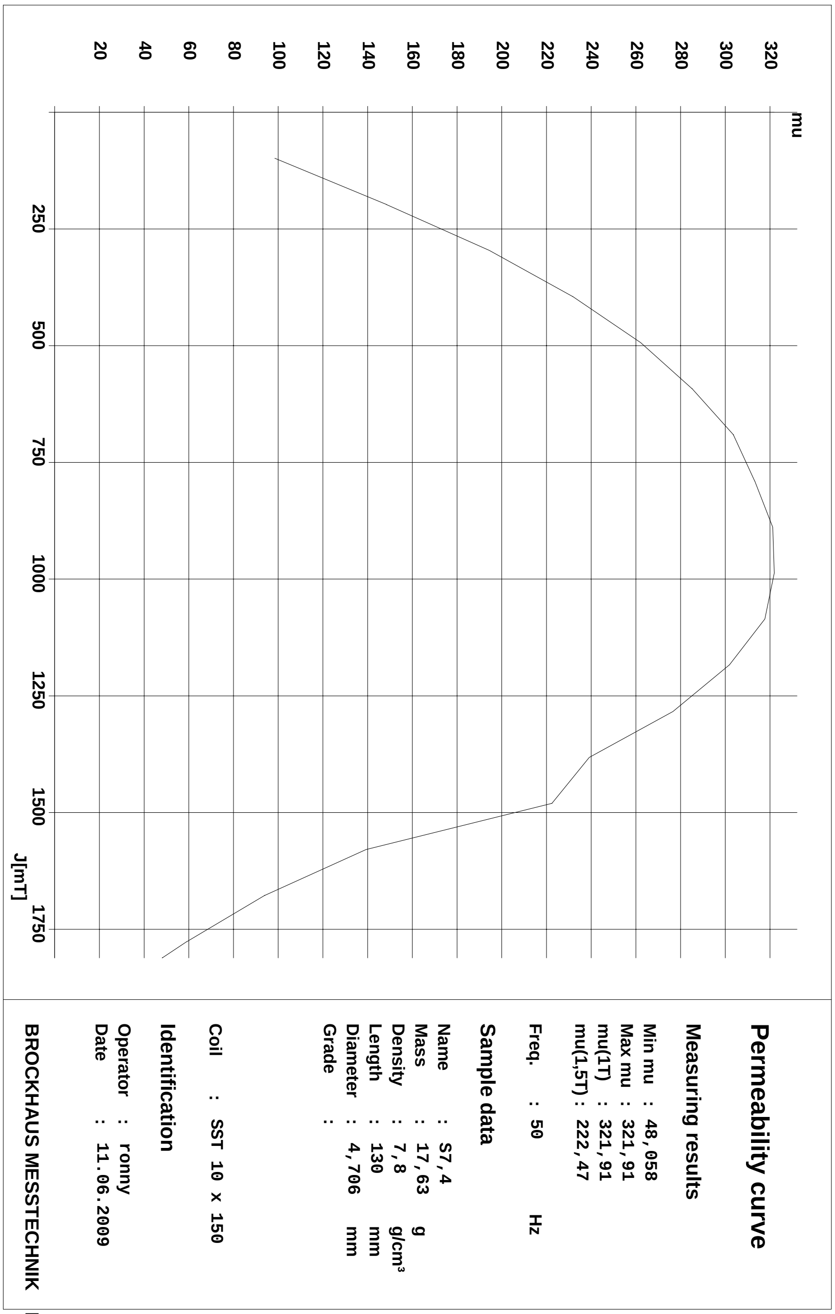

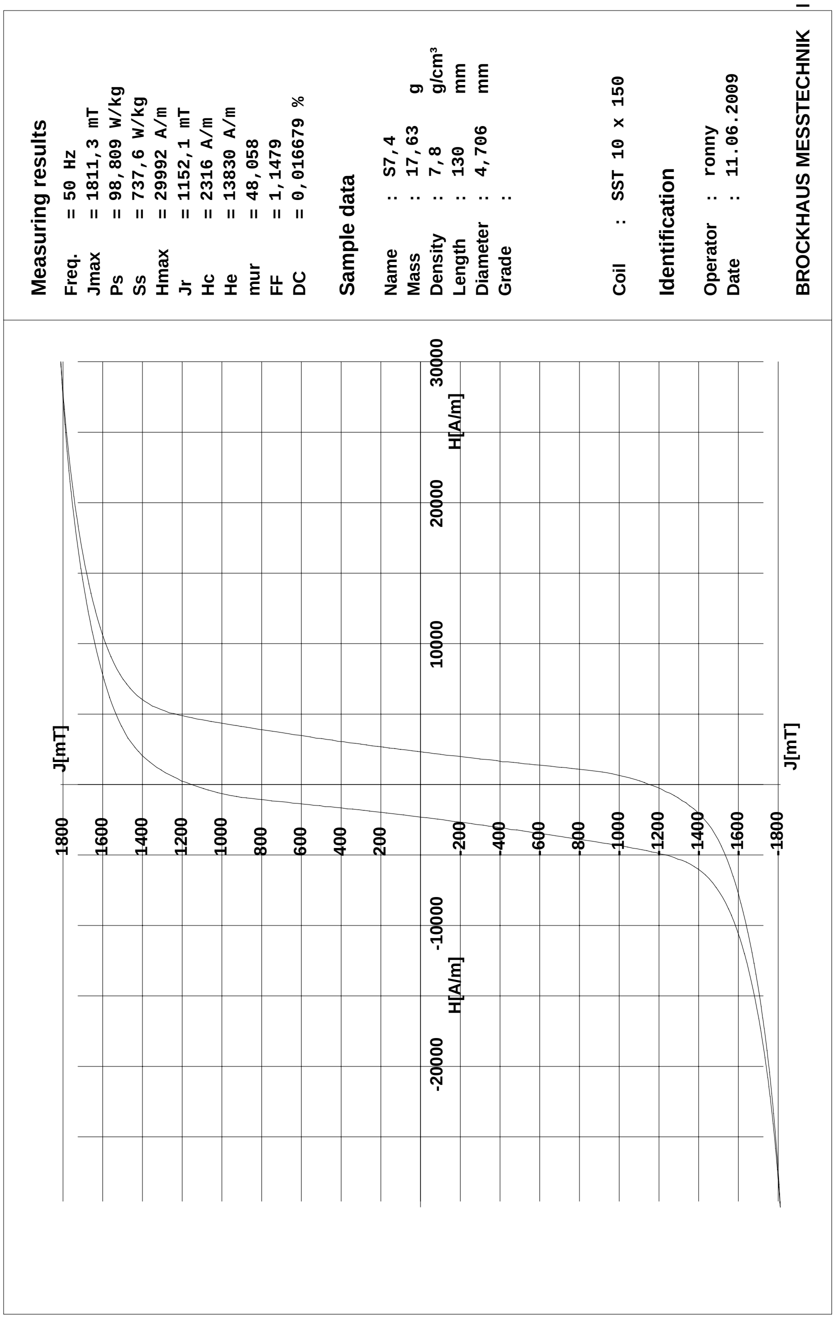
Measuring results
Freq. = 50 Hz
Jmax = 1811,3 mT
Ps = 98,809 W/kg
Ss = 737,6 W/kg
Hmax = 29992 A/m
Jr = 1152,1 mT
Hc = 2316 A/m
He = 13830 A/m
mur = 48,058
FF = 1,1479
DC = 0,016679 %
Sample data
Name : S7,4
Mass : 17,63 g
Density : 7,8 g/cm³
Length : 130 mm
Diameter : 4,706 mm
Grade :
Coil : SST 10 x 150
Identification
Operator : ronny
Date : 11.06.2009
BROCKHAUS MESSTECHNIK
J[mT]
H[A/m]
1800
1600
1400
1200
1000
800
600
400
200
-200
-400
-600
-800
-1000
-1200
-1400
-1600
-1800
30000
20000
10000
-10000
-20000

D.3 Mu Curve and Hysteresis Curve for Sample 2

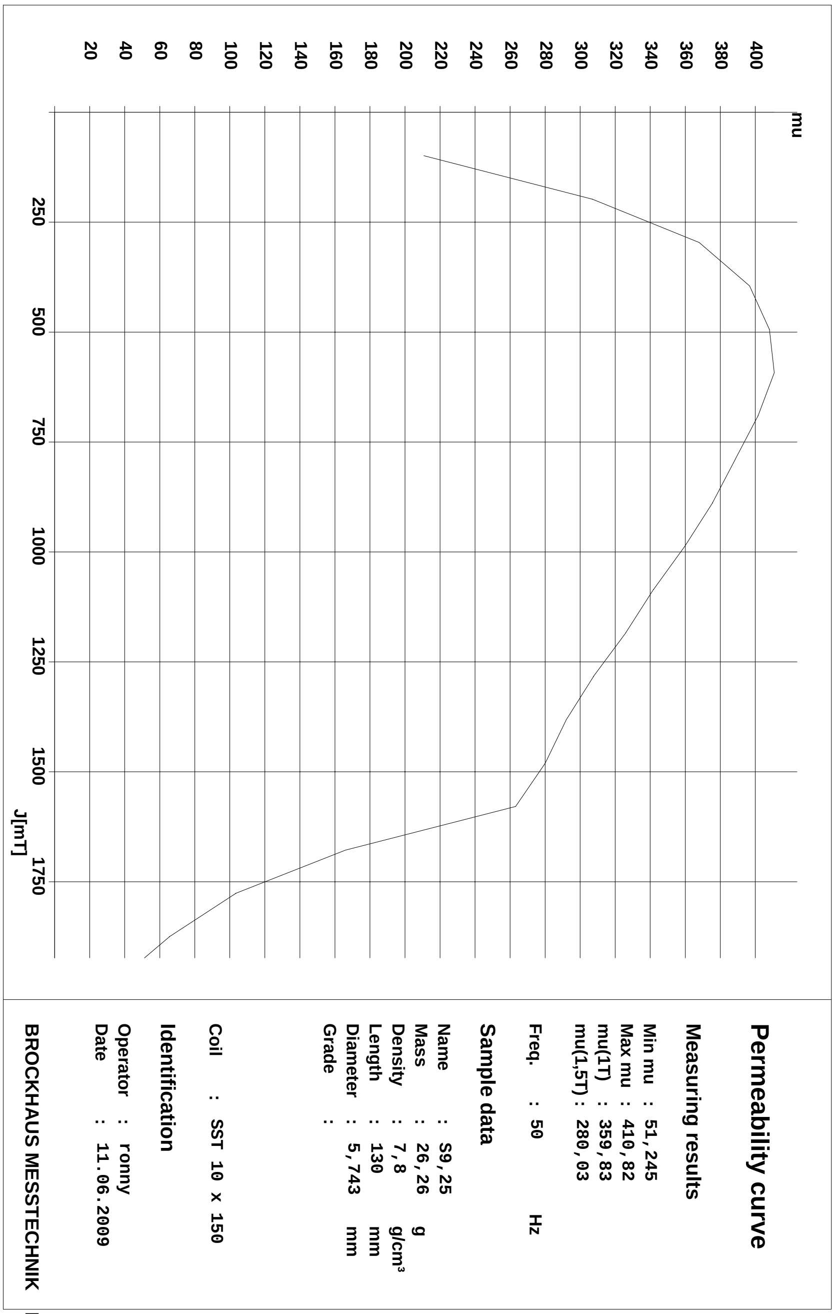

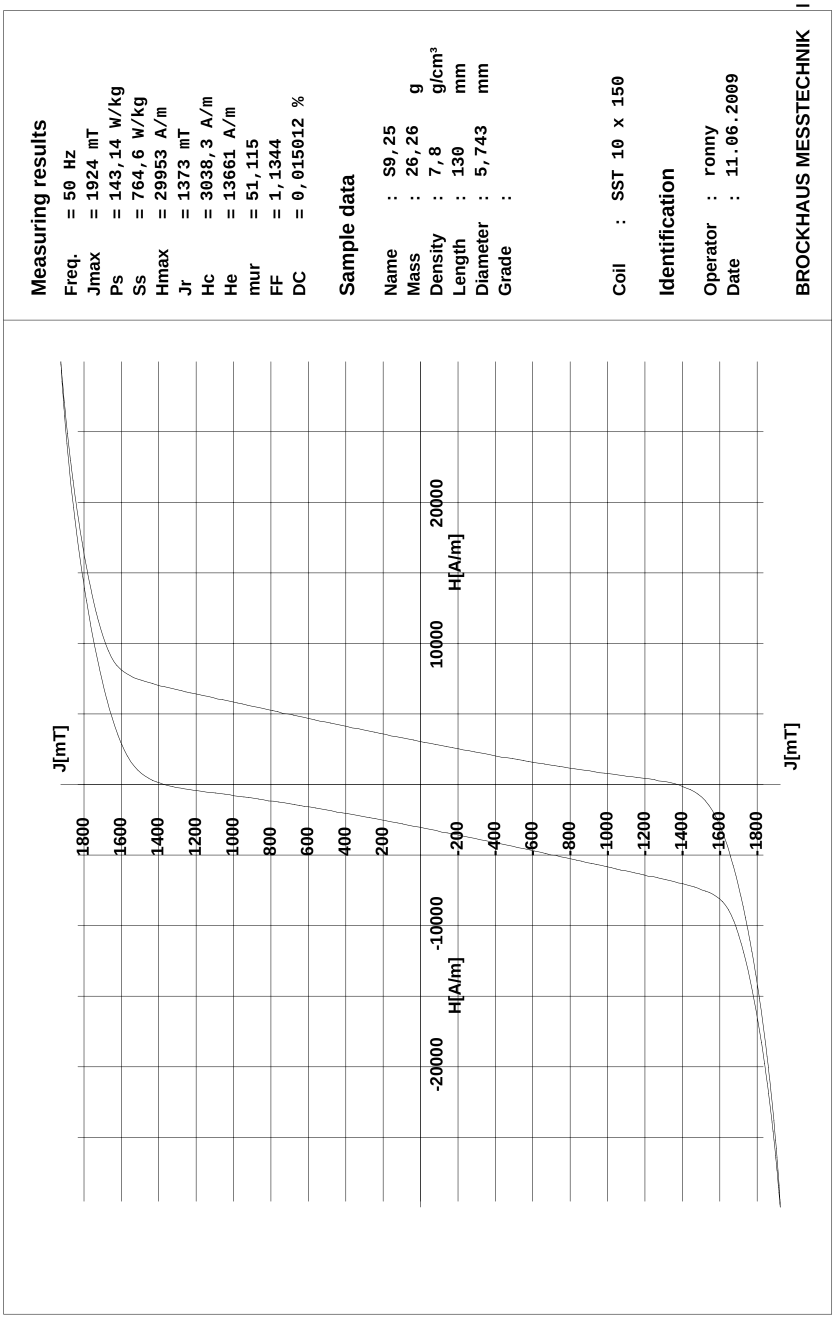
Measuring results
Freq. = 50 Hz
Jmax = 1924 mT
Ps = 143,14 W/kg
Ss = 764,6 W/kg
Hmax = 29953 A/m
Jr = 1373 mT
Hc = 3038,3 A/m
He = 13661 A/m
mur = 51,115
FF = 1,1344
DC = 0,015012 %
Sample data
Name : S9,25
Mass : 26,26 g
Density : 7,8 g/cm³
Length : 130 mm
Diameter : 5,743 mm
Grade :
Coil : SST 10 x 150
Identification
Operator : ronny
Date : 11.06.2009
BROCKHAUS MESSTECHNIK
J[mT]
H[A/m]
20000
10000
-10000
-20000
1800
1600
1400
1200
1000
800
600
400
200
-200
-400
-600
-800
-1000
-1200
-1400
-1600
-1800

D.4 Mu Curve and Hysteresis Curve for Sample 3

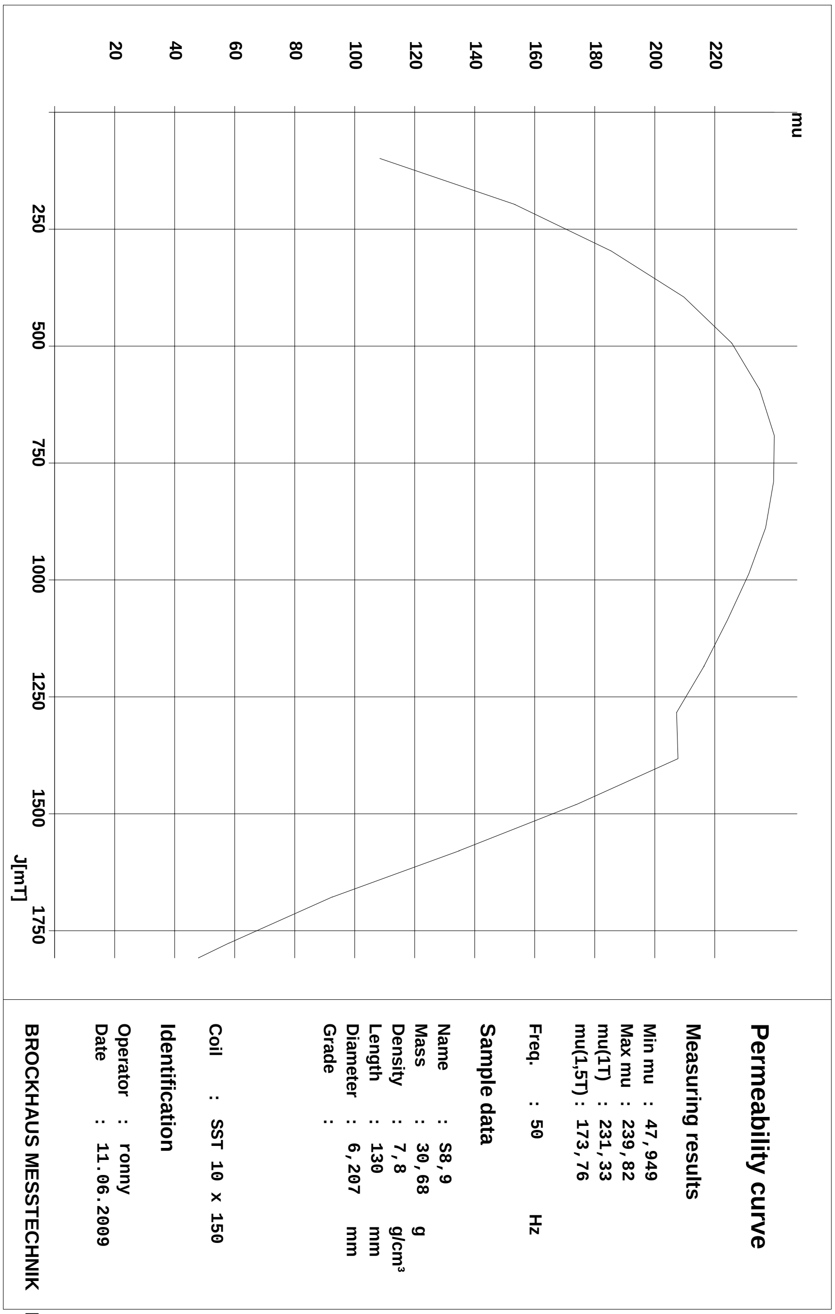

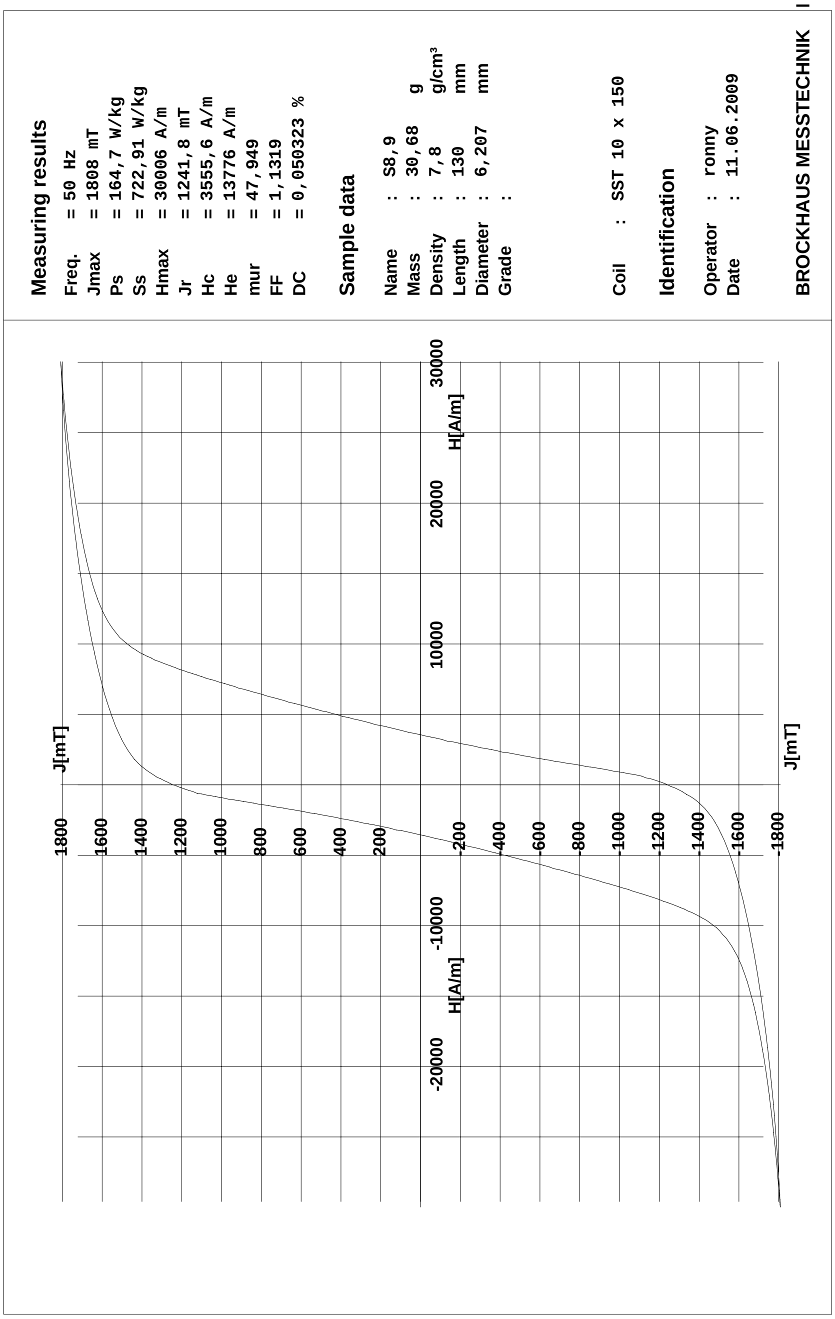
Measuring results
Freq. = 50 Hz
Jmax = 1808 mT
Ps = 164,7 W/kg
Ss = 722,91 W/kg
Hmax = 30006 A/m
Jr = 1241,8 mT
Hc = 3555,6 A/m
He = 13776 A/m
mur = 47,949
FF = 1,1319
DC = 0,050323 %
Sample data
Name : S8,9
Mass : 30,68 g
Density : 7,8 g/cm³
Length : 130 mm
Diameter : 6,207 mm
Grade :
Coil : SST 10 x 150
Identification
Operator : ronny
Date : 11.06.2009
BROCKHAUS MESSTECHNIK
J[mT]
H[A/m]
1800
1600
1400
1200
1000
800
600
400
200
-200
-400
-600
-800
-1000
-1200
-1400
-1600
-1800
30000
20000
10000
-10000
-20000

D.5 Mu Curve and Hysteresis Curve for Sample 4

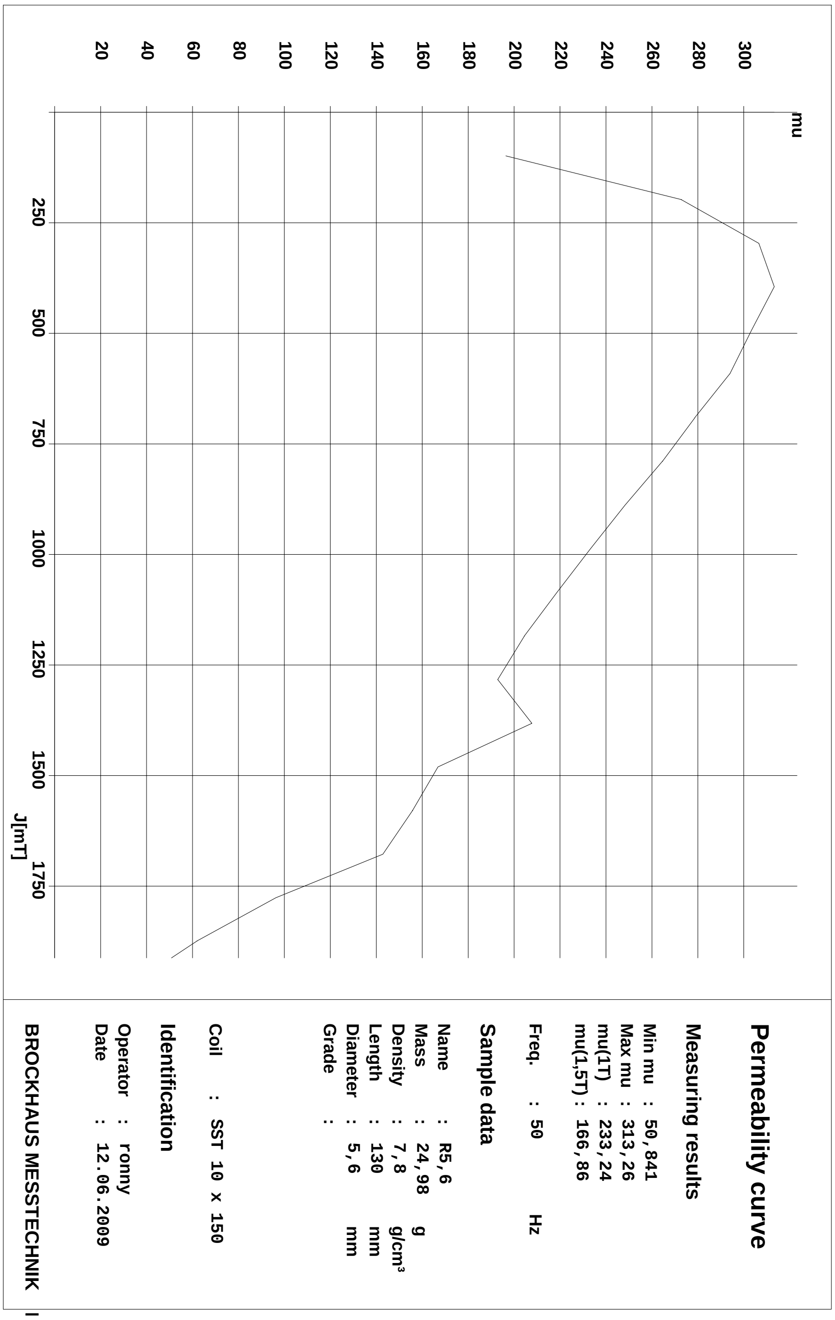

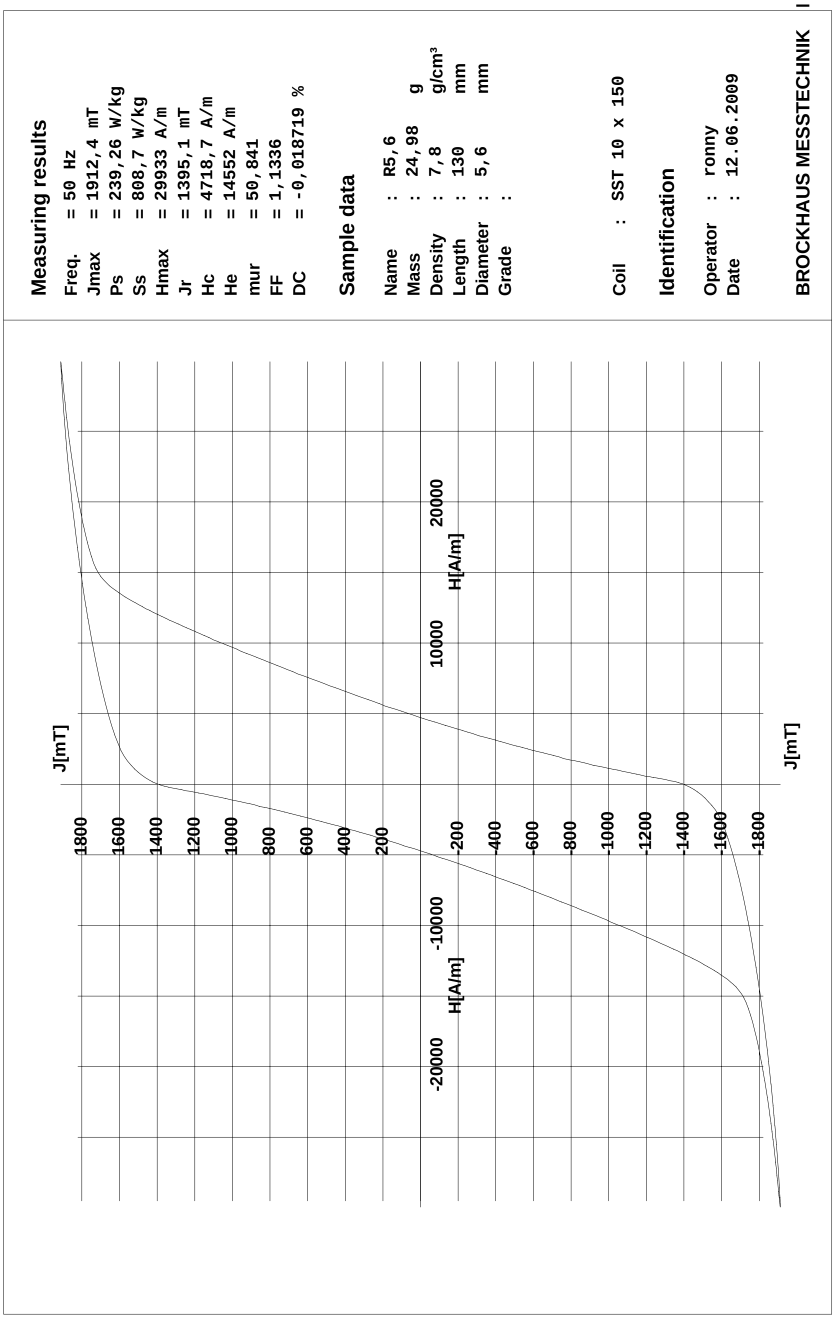
Measuring results
Freq. = 50 Hz
Jmax = 1912,4 mT
Ps = 239,26 W/kg
Ss = 808,7 W/kg
Hmax = 29933 A/m
Jr = 1395,1 mT
Hc = 4718,7 A/m
He = 14552 A/m
mur = 50,841
FF = 1,1336
DC = -0,018719 %
Sample data
Name : R5,6
Mass : 24,98 g
Density : 7,8 g/cm³
Length : 130 mm
Diameter : 5,6 mm
Grade :
Coil : SST 10 x 150
Identification
Operator : ronny
Date : 12.06.2009
BROCKHAUS MESSTECHNIK
J[mT]
H[A/m]
20000
10000
-10000
-20000
1800
1600
1400
1200
1000
800
600
400
200
-200
-400
-600
-800
-1000
-1200
-1400
-1600
-1800